Characterization of Two-Dimensional Oculomotor Control During Goal-Directed Eye Movements in Humans

Vincent Dang
Marquette University

CHARACTERIZATION OF TWO-DIMENSIONAL OCULOMOTOR CONTROL DURING GOAL-DIRECTED EYE MOVEMENTS IN HUMANS

by

Vincent Dang, B.S.

A Thesis submitted to the Faculty of the Graduate School,
Marquette University,
in Partial Fulfillment of the Requirements for
the Degree of Master of Science

Milwaukee, Wisconsin

December 2013

ABSTRACT

CHARACTERIZATION OF TWO-DIMENSIONAL OCULOMOTOR CONTROL DURING GOAL-DIRECTED EYE MOVEMENTS IN HUMANS

Vincent Dang, B.S.

Marquette University, 2013

Oculomotor control is a subset of sensorimotor control that allows humans to make extremely accurate eye movements for ADL. Impairments to oculomotor control can increase the impact of sensorimotor control deficits, especially in neurodegenerative diseases such as MS. Here, a two-dimensional computational control system of saccades and smooth-pursuit eye movements was compiled from literature to systematically characterize oculomotor control in eight visually-healthy humans as a precursor to studying the relationship between oculomotor and sensorimotor control in patient populations.

Subjects visually tracked a single dot on a 41 x 30.5 cm monitor in a dark room while eye positions were recorded at 60 Hz by a video based eye tracker. Data from visual tasks separately consisting of saccades and smooth-pursuit along the horizontal and/or vertical midlines were inputs to an error minimization algorithm that identified individually for each subject the parameters characterizing motor command generation and two-dimensional interactions within ocular dynamics, with bootstrap analysis quantifying the certainty of parameter estimates. Cross-correlation between target and subject gaze positions was used to identify neuronal conduction speeds for saccades and smooth-pursuit processing. A task consisting of small saccades identified the minimum position error required for saccade initiation. A final task combining saccade and smooth-pursuit movements was used to evaluate model performances.

The model accounted for 96% and 98% of variability for subject saccade and smooth-pursuit eye movements, respectively. The 2-D model analysis of saccades and smooth-pursuit identified interactions between horizontal and vertical oculomotor control indicative of component stretching but did not verify the increased speed of vertical versus horizontal eye movements reported in literature. A novel interaction associated with centrifugal curvature was also identified, but the functional effects the interactions were small. Estimated latencies of saccade and smooth-pursuit processing of 242 and 107 ms, respectively, were within ranges provided by literature, while dead zone values for saccade initiation had a 97% error from values provided by literature. The quantitative framework presented in this study may be used in future studies that include MS patients, in which oculomotor control characterization may reveal differences in control strategies for goal-directed ocular movements relative to healthy individuals.

ACKNOWLEDGMENTS

Vincent Dang, B.S.

I am grateful for the Biomedical Engineering Department at Marquette University for granting me an opportunity to perform research as part of the 5-year BS/MS program as well as funding provided through my teaching assistantship. In no particular order, I would also like to thank my parents, siblings, relatives and friends who have given me moral support. I learned that research improves through collaboration, so I thank my committee members and the talented members of Marquette University's Integrative Neural Systems Laboratory for sharing knowledge and feedback on this research. Lastly, I thank Dr. Scott Beardsley for being my research mentor, financial sponsor and comprehensive teacher throughout this entire project.

TABLE OF CONTENTS

ACKNOWLEDGMENTS i

LIST OF FIGURES v

1 INTRODUCTION 1

1.1 Specific Aims 1

1.2 Significance 2

2 BACKGROUND 3

2.1 Eye Movement Types 3

2.2 Saccade Models 3

2.3 Smooth-pursuit Models 6

2.4 Saccade and Smooth-pursuit Interactions 7

2.5 2-Dimensional Relationships between Axial Components 9

2.6 System identification of Oculomotor Control 11

3 METHODS 13

3.1 2-D Oculomotor Control Model 13

3.1.1 Overall Control Scheme 13

3.1.2 Saccade Loop 19

3.1.3 Smooth-pursuit Loop 20

3.2 Subjects 21

3.3 Experimental Materials/Setup 22

3.4 Visual Tasks 23

3.4.1 Saccade Task 24

3.4.2 Smooth-pursuit Task 25

3.4.3 Combined Saccade and Smooth-pursuit Task 26

3.4.4 Saccade Threshold Task 27

3.5 Data Analysis 27

3.5.1 Data Preprocessing 27

3.5.2 Initial-Model 28

3.5.3 System Identification 31

3.5.4 Bootstrap Analysis 36

4 RESULTS 39

4.1 Analyses Prior to Model Fitting 39

4.1.1 Delay Analysis 39

4.1.2 Dead Zone Analysis 41

4.1.4 Accuracy and Precision Analysis 43

4.2 Parametric Analysis 46

4.2.1 Saccade Controllers 46

4.2.2 Smooth-pursuit Controllers 49

4.2.3 2-D Interaction Parameters 54

4.3 Model Performance Evaluation 64

4.3.1 Model Performance without Delay Estimations 65

4.3.2 Model Performance with Delay Estimations 66

5. DISCUSSION 68

5.1 Delay and Dead zone Analyses 68

5.1.1 Delay Estimates 68

5.1.2 Dead Zone Estimates 70

5.2 Parametric Analysis 70

5.2.1 Initial-Model 70

5.2.2 Saccade Control 71

5.2.3 Smooth-Pursuit Control 74

5.2.4 2-D Interaction Control 76

5.3 Model Limitations 80

5.4 Future Directions 83

5.4.1 Improving Eye Movement Characterization 83

5.4.2 Eye Movement Studies in Persons with Multiple Sclerosis 88

6. CONCLUSION 90

BIBLIOGRAPHY 91

LIST OF FIGURES

FIGURE 1: SACCADE MAIN SEQUENCE CURVE (BAHILL, 1975). 4

FIGURE 2: INTERACTIONS BETWEEN SACCADE AND SMOOTH-PURSUIT SYSTEMS (ORBAN DE XIVRY & LEFEVRE, 2007). 8

FIGURE 3: 2-D OCULOMOTOR CONTROL MODEL 14

FIGURE 4: MODEL OUTPUTS SHOWING THE EFFECT OF DRIFT COMPENSATION 19

FIGURE 5: EXPERIMENTAL SETUP (WAKDE, 2011) 23

FIGURE 6: SACCADE AND SMOOTH-PURSUIT CONTROLLER OUTPUTS USING THE INITIAL-MODEL, COMPARED TO SUBJECT EYE MOVEMENTS FROM PILOT DATA 29

FIGURE 7: MAIN SEQUENCES FOR SACCADES AND SMOOTH-PURSUIT EYE MOVEMENTS. 31

FIGURE 8: WORKFLOW FOR SYSTEM IDENTIFICATION PROCESS 32

FIGURE 9: PARAMETER SPACE FOR 2ND STAGE FITTING TO A SINGLE PARAMETER 35

FIGURE 10: AVERAGE SACCADE AND SMOOTH-PURSUIT LATENCIES ACROSS TRIALS 40

FIGURE 11: TASK-DEPENDENT LATENCIES AVERAGED ACROSS ALL SUBJECTS. 40

FIGURE 12: EXAMPLE TIME-SERIES FROM A TYPICAL SUBJECT (EM_S03) 42

FIGURE 13: SAMPLE FIT TO THE HORIZONTAL SACCADE TASK FOR (EM_S03). 47

FIGURE 14: SAMPLE FIT TO THE VERTICAL SACCADE TASK FOR (EM_S03). 48

FIGURE 15: BOX-COXED TRANSFORMED MEAN OF SACCADE CONTROLLER GAINS ACROSS SUBJECTS 49

FIGURE 16: SAMPLE FIT TO THE HORIZONTAL SMOOTH-PURSUIT TASK (EM_S03). 50

FIGURE 17: SAMPLE FIT TO VERTICAL SMOOTH-PURSUIT TASK (EM_S03) 51

FIGURE 18: AVERAGE PARAMETER ESTIMATES ACROSS SUBJECTS FOR SMOOTH-PURSUIT CONTROLLER GAINS 52

FIGURE 19: PID GAINS FOR THE BEST-FIT SMOOTH-PURSUIT (SP) CONTROLLERS ACROSS SUBJECTS. 52

FIGURE 20: SAMPLE TIME-SERIES FOR VERTICAL SMOOTH-PURSUIT MOVEMENTS FOR SUBJECTS EM_S09 AND EM_S05 53

FIGURE 21: DISTRIBUTIONS OF BEST-FIT SYSTEM INTERACTION PARAMETERS FOR EM_S03 USING THE 2-D SACCADE TASK 58

FIGURE 22: DISTRIBUTIONS OF BEST-FIT ERROR-DRIVEN SYSTEM INTERACTION PARAMETERS FOR EM_S03 USING THE 2-D SACCADE TASK 58

FIGURE 23: DISTRIBUTIONS OF BEST-FIT SYSTEM INTERACTION PARAMETERS FOR EM_S03 USING THE 2-D SMOOTH-PURSUIT TASK 59

FIGURE 24: DISTRIBUTIONS OF BEST-FIT ERROR-DRIVEN SYSTEM INTERACTION PARAMETERS FOR EM_S03 USING THE 2-D SMOOTH-PURSUIT TASK 60

FIGURE 25: EFFECTS OF 2-D SYSTEM INTERACTIONS ON SACCADE RESPONSE FOR EM_S09. 60

FIGURE 26: EFFECTS OF 2-D SYSTEM INTERACTIONS ON SMOOTH-PURSUIT RESPONSE FROM EM_S09. 61

FIGURE 27: GOODNESS OF FITS FOR 2-D INTERACTION PARAMETERS UNDER TRAINING DATA FOR SACCADE DATA AND SMOOTH-PURSUIT DATA. 62

FIGURE 28: SAMPLE SUBJECT (EM_S06) AND MODEL RESPONSES FROM THE COMBINED SACCADE AND SMOOTH-PURSUIT TASK 63

FIGURE 29: MODEL VALIDATION USING SUBJECT-SPECIFIC BEST-FIT MODELS WITH TEST DATA. 65

FIGURE 30: SAMPLE TIME-SERIES FROM 2-D DUAL-MOVEMENT TASKS FOR MODEL VALIDATION WITH DELAYS INCLUDED. 66

FIGURE 31: SAMPLE TIME-SERIES (EM_S09) FOR 1-D HORIZONTAL AND VERTICAL SACCADES. . 73

FIGURE 32: INTERACTION EFFECTS WITHIN THE SYSTEM BASED SOLELY ON POSITION FROM THE 2-D SACCADE TASK OF A SAMPLE SUBJECT (EM_S08). 77

FIGURE 33: COMPARISON OF PULSE-STEP VS. PD SACCADE CONTROL 85

FIGURE 34: EFFECT OF INCREASING MOTOR COMMAND SATURATION ON PULSE-STEP CONTROL. 87

1 INTRODUCTION

Sensorimotor control is characterized by the use of sensory information (visual, auditory, tactile and proprioceptive) to control movements, including those required for activities of daily living (ADL). The field of oculomotor control studies the use of sensory information in the control of goal-directed eye movements, which are extremely accurate compared to limb movements. Computational models have been developed to emulate eye movements using control systems that incorporate eye dynamics, sensory feedback, neuronal conduction speeds and motor command generation. Impairments to oculomotor control can increase the impact of sensorimotor control deficits by providing inaccurate visual feedback during goal-directed tasks. Understanding how deficits in oculomotor control contribute to impairments in goal-directed arm movements is important in neurodegenerative diseases such as Multiple Sclerosis (MS). Systematically characterizing an individual's oculomotor control mechanisms is a precursor to studying this relationship. The goal of this study is to characterize oculomotor control in a cohort of healthy subjects. Three specific aims will be addressed.

1.1 Specific Aims

1. Develop a model of oculomotor control and characterize its response to saccade and smooth-pursuit eye movements based on published literature.
2. Apply system identification techniques to characterize experimentally the oculomotor control model for individual subjects and evaluate the model performance in response to saccades and smooth-pursuit eye movements.

3. Characterize position and velocity-based interactions between horizontal and vertical oculomotor control during oblique eye movements in neurologically intact subjects.

1.2 Significance

Many studies of eye movement deficits focus on characterizing deficit features to more clearly define and detect them. The use of oculomotor control models provides a theoretical framework to relate the features of eye movement deficits to specific functional and/or computational sources of impairment. In work presented here, a model of 2D oculomotor control is developed based on the literature and evaluated in terms of its stability and accuracy in modeling eye movements of visually healthy subjects. The model's stability was evaluated based on replication of a well-known velocity-based characteristic for eye movements, and the accuracy was evaluated based on detection of known features in two-dimensional eye movements. Successful implementation of this model, and the methodology required to characterize it based on individual subject data, will provide a quantitative framework for characterizing the functional source(s) of impairment that contribute to oculomotor deficits and their contribution to impairments in goal-directed arm movement. At that point, inferences may be made about the functional source(s) of the deficits by understanding what control element(s) can account for the deficit-induced movements. In addition, this model may be sensitive to effects in oculomotor control not previously described in the literature, such as interactions between horizontal and vertical eye dynamics. Thus, this study provides methodology for future patient studies while further characterizing oculomotor control in healthy subjects.

2 BACKGROUND

2.1 Eye Movement Types

Models of the oculomotor system typically characterize 4 types of eye movements: saccades, smooth-pursuit, vergence and vestibular-ocular reflex (VOR) movements. Saccades are used for ADL such as reading and scanning the environment, and are characterized by rapid, jerky movements, with speeds up to 1000˚/second, durations ranging 30-80 ms and latencies between movements of 200-250 ms (Abrams, Meyer, & Kornblum, 1989; Robinson, 1964; Thomas, 1969; Westheimer, 1954). Smooth-pursuit movements occur during voluntary tracking of moving targets with speeds up to 100˚/second and latencies of about 100 ms (Meyer, Lasker, & Robinson, 1985; Purves, 2001). Vergence eye movements occur when the oculomotor system fixates targets in depth, resulting in opposite motion between eyes. VOR movements are reflexive and used to maintain fixation on a target in response to head movements (Purves, 2001).

2.2 Saccade Models

Some eye movement control models are typically characterized by saccadic eye movements. A variety of models have been developed to characterize saccades (Bahill, Clark, & Stark, 1975a; Becker & Jurgens, 1990; Chen-Harris, Joiner, Ethier, Zee, & Shadmehr, 2008; Clark & Stark, 1976; G.; Cook & L. Stark, 1968; Freedman & Cecala, 2008; Grossman & Robinson, 1988; van Gisbergen, van Opstal, & Schoenmakers, 1985; L. R. S. Young, L, 1963) including the quasi-linear relationship between saccade peak velocity and amplitude for saccades smaller than 20˚ (A. T. C. Bahill, M.R.; Stark, L,

1975). This effect is characterized by saturation of the peak velocity curve with saccade magnitude, referred to as the main sequence, for saccades larger than 20˚ (A. T. C. Bahill, M.R.; Stark, L, 1975).

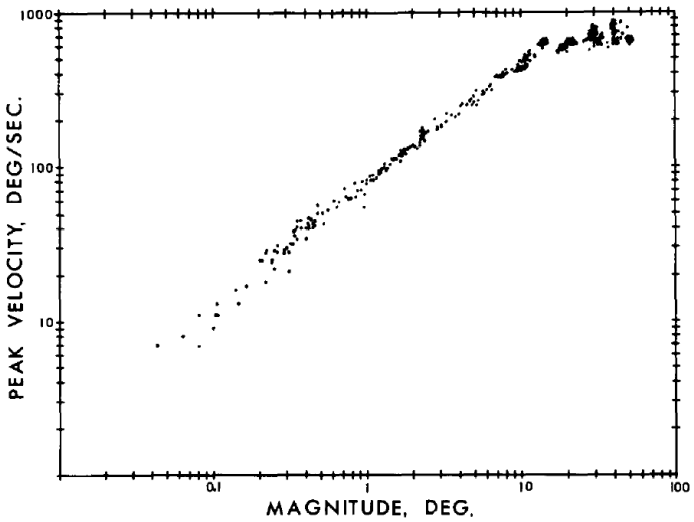

Figure 1: Saccade Main Sequence curve (Bahill, 1975). Peak velocity during a saccade increases linearly with saccade magnitudes for small and medium eye displacements (<20˚). For saccades greater than 20˚, peak velocity saturates.

Head-restrained models of goal-directed saccades generally simulate oculomotor control as a closed-loop process for multiple saccades characterized by a controller, comparing current eye position with target location, a signal transduction and ocular muscle dynamics (Becker & Jurgens, 1990; Chen-Harris et al., 2008; Freedman & Cecala, 2008; Nichols & Sparks, 1996; van Gisbergen et al., 1985). Six ocular muscles actuate each human eye and can be modeled individually as mass-spring-damper systems. Previous studies have shown the resultant dynamics of the eye during rotation about a single axis can be approximately accounted for by a 2^{nd} order system whose inertia, friction and elasticity can be collectively characterized by time constants of 224 and 13 ms (Robinson, Gordon, & Gordon, 1986). Saccade models accounting for nerve input

are important for understanding the input-output signal transduction of the visual system, but the nerve input encodes visual target location and is commonly replaced by visual target input for models focusing only on control characteristics.

Saccade control models assume an open-loop response for single saccades because saccade duration (30-80 ms) is shorter than the delay associated with the visual feedback (200 ms), resulting in an all-or-nothing response to the displacement of a visual target. The response is typically modulated by a short burst signal (pulse) to provide the high saccade velocity followed by a longer tonic signal (step) to hold eye position, both of which comprise the pulse-step controller (Bahill, Clark, & Stark, 1975b). Following a primary ballistic saccade, error-corrective eye movements have been shown to undershoot the target (Kapoula & Robinson, 1986), consistent with a negative feedback closed-loop control process. Closed-loop control is also required to account for sequential saccades, where an efference copy of the motor command is typically used together with an internal representation of the ocular plant to predict the consequences of a motor command on eye position in the absence of visual feedback (Bridgeman, 2007; Chen-Harris et al., 2008; Miall, Weir, Wolpert, & Stein, 1993). This signal is compared to target position to give a predictive error signal, accounting for the high accuracy and speed of saccades.

Nonlinear saccade models focusing on the discrete nature of saccades have incorporated a sampler with a 200 ms duration and a dead zone of ±0.5˚ (L. R. S. Young, L, 1963). The sampler limits the oculomotor system output to one saccade within a duration window corresponding to the duration of a typical saccade to prohibit a new saccade from interrupting a current saccade. The sampling zone enables visual

information processing by preventing saccades when the target is projected sufficiently onto the fovea.

2.3 Smooth-pursuit Models

During continuous movement of a visual target, the oculomotor system uses smooth-pursuit eye movements to place the target on the fovea as accurately as possible. In contrast to saccade models which operate on the position error, smooth-pursuit models aim to reduce retinal slip, or the velocity error between the target and the eye (Forster, Van Houtte, & Young, 1969; Lisberger, Evinger, Johanson, & Fuchs, 1981; Robinson et al., 1986; L. R. Young, 1971)Depending on the type of movement, these models may involve target prediction. For example, when presented with a sinusoidal, predictive target, the smooth-pursuit system can extrapolate future target positions to emulate physiological zero-latency tracking using a target menu-selection method, which identifies the target movement as one from a set of pre-defined movement types (Bahill & McDonald, 1983). Other models disregard this physiological phenomenon assuming that an encounter with a predictive continuous target is rare (Lisberger et al., 1981; Robinson et al., 1986). Despite not always showing zero-latency tracking, smooth-pursuit eye movements are advantageous over saccades in that the latency, ~100 ms, for initiation of a smooth pursuit movement is approximately half of the saccade latency (Orban de Xivry & Lefevre, 2007).

More so than in saccade models, smooth-pursuit models place an emphasis on nonlinearities in order to model smooth-pursuit characteristics. Traditionally a position-based dead zone has not explicitly been a part of smooth-pursuit models as the positional error has been regarded as irrelevant for a velocity-driven system. For velocity-driven

systems, two nonlinearities are typically considered: a rate limiter of about ±70 degrees/seconds to prohibit response to high-velocity targets, and velocity saturation of about ±60 degrees/seconds to model physiological limitations on smooth-pursuit eye movement speed (Bahill & McDonald, 1983). These nonlinearities are modeled after smooth-pursuit dynamics observed experimentally and typically act in conjunction with a second order controller in a feed-forward path. Similar to the saccade models, these models incorporate an internal feedback loop to minimize error in the absence of visual feedback. However, because smooth-pursuit relies more heavily on visual feedback, especially for unpredictable targets, the closed loop nature of the control system plays a more prominent role in reducing the overall error, compared to saccade control.

2.4 Saccade and Smooth-pursuit Interactions

Smooth-pursuit is rarely observed without some saccade interaction. During a visual tracking task, catch-up saccades compensate for excessive positional error due to velocity constraints in the execution of a smooth-pursuit movement (Orban de Xivry & Lefevre, 2007). Unlike saccades made to discrete targets, catch-up saccades consider velocity error to predict and compensate for the low velocity of a smooth-pursuit command (de Brouwer, Yuksel, Blohm, Missal, & Lefevre, 2002). The disadvantage of fast error-correction with catch-up saccades is that vision is lost for the duration of the saccade, as the high velocity movement negates the eye's ability to maintain the target on the fovea. Due to the trade-off between poor vision and poor tracking when considering use of catch-up saccades, its use may vary based on the complexity of the tracking tasks (Orban de Xivry & Lefevre, 2007).

The interaction between saccades and smooth-pursuit can be accounted for by the use of a dual-movement model (Young & Stark, 1963; de Brouwer et al., 2002). In the model, the smooth-pursuit system is continuously activated during target tracking, while the saccade system only generates a motor command when the eye-crossing time exceeds 140 ms, or the positional error exceeds the dead zone (Young & Stark, 1963; de Brouwer et al., 2002). The eye-crossing time, T_{XE}, is an artificial parameter defined as the time calculated for the eye to coincide with the target at constant eye velocity, (Equation 2.1), where PE and RS are position error and retinal slip, respectively (de Brouwer et al., 2002). If the eye-crossing time or dead zone output is such that both subsystems output

$$T_{XE} = -\frac{PE}{RS} \qquad (2.1)$$

a motor command, the commands are summed before actuating the ocular plant. Figure 2 shows a block diagram representation of the proposed interaction of the two subsystems.

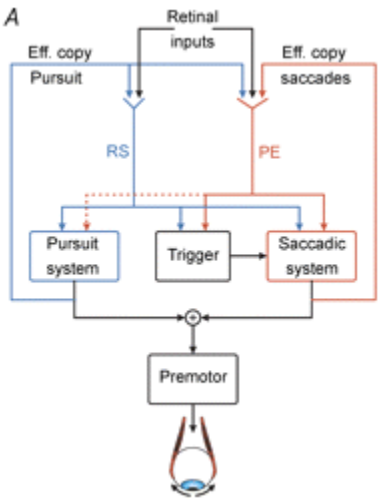

Figure 2: Interactions between saccade and smooth-pursuit systems. Positional error and velocity based errors (retinal slip) influence the motor command output of both subsystems and the trigger, which is a binary signal enabling a saccade output. The dashed orange line indicates the influence of positional error on smooth-pursuit is based only on partial evidence, as it has been difficult to disassociate positional errors from persistent velocity based errors for smooth-pursuit experiments. Efference copies, which are neurological copies of the motor command signal, of the saccade and smooth-pursuit subsystems are compared with the retinal inputs encoding target position to compute positional and velocity based errors respectively, with the smooth-pursuit efference copy additionally

influencing the computation of positional error. Regardless of the state of the trigger signal, the outputs of the two subsystems are continuously summed to provide the motor command to the eye (Orban de Xivry & Lefevre, 2007).

2.5 2-Dimensional Relationships between Axial Components

Oculomotor models have been extended to the 2-D plane to characterize control during vertical and oblique eye movements. Historically, horizontal eye movement studies in humans have dominated the literature due to their behavioral prominence in daily activities and in part to eyelid interference during vertical eye movements. Despite the relative recentness of oblique eye movement studies, one quantitative property of human oblique saccades has been well established: component duration stretching to reduce (but not eliminate) saccade curving (Becker and Jurgens 1989, Smit 1990). Component stretching increases the duration of the component with a smaller amplitude and is used to synchronize the end time of the axial components during an oblique saccade. For example, an oblique saccade traveling 10˚ horizontally and 5˚ vertically may decrease vertical velocity to synchronize movement end times across axes. Reported in 40% of oblique saccades, the mechanism for duration stretching includes glissades (smooth gliding movement), dynamic overshoot and multiple saccades to reach the target (A. T. S. Bahill, L, 1975). It should be noted that 1-D curvature, defined by inconsistencies in velocity throughout the movement profile, was shown in models that use pulse-step controllers to modulate saccades (Bahill et al., 1975b).

One hypothesis for interaction between the horizontal and vertical eye movements is independent feedback control, defined as independent generations of motor commands for horizontal and vertical eye movements where the horizontal error feedback does not influence the vertical eye movements (and *vice versa*), ensuring the magnitudes of the

motor commands are simply not scalars of one another as proposed by a contrasting hypothesis known as vectorial comparator control (Nichols & Sparks, 1996). Recent studies using head movements and electrical stimulation of the Superior Colliculus have shown that the independent feedback control model more accurately accounts for oblique saccade characteristics compared to the vectorial comparator control model (Nichols & Sparks, 1996; Freedman & Cecala, 2008).

Another hypothesis for 2-D interaction control is known as the mutual-coupling hypothesis (Becker & Jurgens, 1990; Grossman & Robinson, 1988). Grossman and Robinson proposed that the position output of one component attenuates the gain of its orthogonal component (Grossman & Robinson, 1988). Becker and Jurgens suggested a cross-coupling of the horizontal and vertical motor errors as shown in Equations 2.2 and 2.3 (Becker & Jurgens, 1990). Both equations show that the magnitude of the position in horizontal or vertical eye movements attenuates the velocity of the orthogonal component, where pos_h, pos_v, vel_h, vel_v, and c respectively represent the horizontal position, vertical position, horizontal velocity, vertical velocity and a tuning coefficient

$$vel_h = \frac{pos_h}{(1 + c \cdot pos_v)} \tag{2.2}$$

$$vel_v = \frac{pos_v}{(1 + c \cdot pos_h)} \tag{2.3}$$

that is typically fit to experimental data as a positive value (Becker & Jurgens, 1990). Both of these mechanisms incorporate positional cross-coupling between the two orthogonal control components. To our knowledge, velocity-based error has not been

tested as a contributor to component stretching in oblique saccades. The influence of velocity-based error towards 1-D control of eye movements has been shown in previous studies (Orban de Xivry & Lefevre, 2007), so it is reasonable to believe that this error type could influence 2-D control if 2-D control retains control mechanisms from 1-D control sub-systems. System interactions between horizontal and vertical eye movements such as centrifugal curving (Becker & Jurgens, 1990) and vertical position offset as a function of horizontal eccentricity (A. T. S. Bahill, L, 1975), have been shown qualitatively and provide context for investigating quantitatively the 2-D interactions between horizontal and vertical oculomotor control.

2.6 System identification of Oculomotor Control

Previous efforts have been made to model normative saccade and/or smooth-pursuit control systems and acquire typical control characteristics across subjects (Chen-Harris et al., 2008; Clark & Stark, 1976; Freedman & Cecala, 2008; Quaia & Optican, 1997; Robinson et al., 1986; L. R. S. Young, L, 1963). However, few of these normative models have been used to distinguish characteristics between subjects, which can be important for studying heterogeneous patient populations such as MS. Existing studies using system identification has been used to characterize oculomotor control in non-human systems such as humanoid vision systems (Schmidt-Cornelius, 2002). Studies motivated by human physiology have used oculomotor control models to describe neurological deficits, such as those in Duane-Syndrome or Progressive Supranuclear Palsy, but these have been limited to either 1-dimensional movement or a single type of movement (saccade or smooth-pursuit) (Helmle, Jahn, & Bille, 1983;

Schneider et al., 2011). Models capable of characterizing a wider array of movement types may be more representative of typical oculomotor control, since eye movements to everyday targets are rarely exclusively saccade, smooth-pursuit or 1-D. Identification of these models in individuals could provide greater insights into oculomotor control strategies and how their impairment impacts other forms of goal-directed movements.

3 METHODS

3.1 2-D Oculomotor Control Model

The proposed oculomotor control model characterizes two types of eye movement, saccades and smooth-pursuits, to constrain the number of variables in the model and improve curve-fitting. Saccades and smooth-pursuit movement were chosen because of their presence in oculo-manual relationships, particularly the influence of eye movement control on arm movement control, seen in goal-directed movements (Feys et al., 2008; Feys, Helsen, Lavrysen, Nuttin, & Ketelaer, 2003; Feys, Helsen, Liu, et al., 2003; Feys et al., 2005; Vercher, Quaccia, & Gauthier, 1995). The impact of Vergence and VOR movements were reduced in the experimental design by avoiding 3-D stimuli and using a forehead and chin rest to minimize head movement.

The model was implemented using MATLAB's Systems Identification toolbox. As a nonlinear grey box model, our model structure was built into a separate file, similar to a function, with 54 parameters. Twelve parameters were dependent on others and ten parameters were obtained through non-parametric analysis, resulting in 32 unique parameters obtained through system identification. Code within the model file represents the model block diagram (Figure 3).

3.1.1 Overall Control Scheme

Figure 3 shows a block diagram of the oculomotor control model used in this study. The multiple input, multiple output model receives visual input about target position in the horizontal and/or vertical plane, and adjusts the eye position to fixate on the target. The model contains separate control paths, one for saccade and one for

smooth-pursuit, that combine to provide corrective motor command to the eye. The outermost feedback path compares the current eye position to the target input to compute a position error which drives the system.

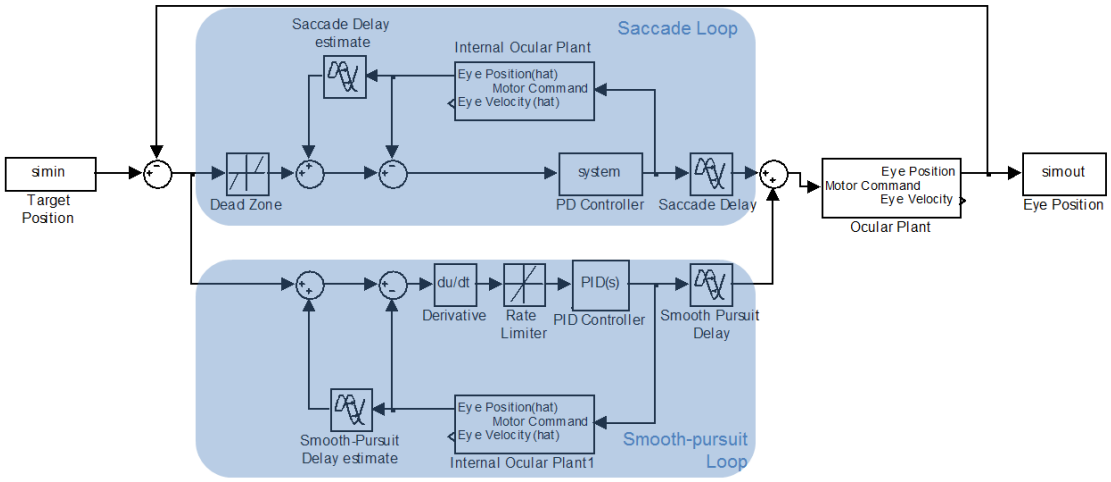

Figure 3: 2-D Oculomotor Control Model. The input and output signals are comprised of horizontal and vertical components of the target and eye positions, respectively. Saccade generation is mediated by the top forward and feedforward paths, while smooth-pursuit generation is mediated by the bottom paths. Each control path incorporates an internal model to generate a predictive error signal to minimize error and response time. The largest loop compares the eye position to the target to generate an actual error signal that drives the system. The ocular plant is a 2nd order system characterizing inertia, friction and elasticity of the eyeball.

The model assumes that smooth-pursuit eye movement control is continuously enabled, and saccade control is discretely enabled. The two system's motor commands are always summed, even if saccade control is momentarily disabled. It should be noted that the output of the saccade control path is typically much larger than that of the smooth-pursuit control path for tasks with larger discrete target movement, resulting in insignificant difference between the sum of the two motor commands and the saccade command.

The position error relative to the target forms the input to the saccade and smooth-pursuit control loops. The outputs from the loops are summed to form the motor

command and used to actuate a second order model of the eye dynamics, proposed by Chen-Harris (Chen-Harris et al., 2008). Earlier smooth-pursuit models approximated the

$$P(s) = \frac{1}{(T_1 s + 1)(T_2 s + 1)} \tag{3.1}$$

ocular plants as a dual lag system (P(s)) where T_1 and T_2 are time constants of 224 ms and 13 ms (Robinson et al., 1986). This model assumes that antagonistic muscle actuator dynamics in each direction is lumped into a single passive plant driven by an implicit differential drive. In the current model, the continuous time transfer function was transformed to a state-space representation with horizontal and vertical eye

$$\dot{x} = Ax + Bu \tag{3.2}$$

$$y = Cx + Du \tag{3.3}$$

position and velocity as the state variables (Equations 3.2 and 3.3), where *x*, *u* and *y* correspond to the state variables, inputs and outputs in vector form, and *A*, *B*, *C* and *D* correspond to state, input, output and feedforward matrices respectively. The system and input matrices were discretized by computing the state transition, or matrix exponential, of the system using a step size of 16 ms based on the 60 Hz resolution of the eye tracking system, resulting in a 2 input / 2 output model characterizing eye position, where the

$$\begin{bmatrix} pos_h(t+1) \\ vel_h(t+1) \\ pos_v(t+1) \\ vel_v(t+1) \end{bmatrix} = \begin{bmatrix} A_{1h} & A_{2h} & A^{v-pos}{}_{h-pos} & A^{v-vel}{}_{h-pos} \\ A_{3h} & A_{4h} & A^{v-pos}{}_{h-vel} & A^{v-vel}{}_{h-vel} \\ A^{h-pos}{}_{v-pos} & A^{h-vel}{}_{v-pos} & A_{1v} & A_{2v} \\ A^{h-pos}{}_{v-vel} & A^{h-vel}{}_{v-vel} & A_{3v} & A_{4v} \end{bmatrix} \begin{bmatrix} pos_h(t) \\ vel_h(t) \\ pos_v(t) \\ vel_v(t) \end{bmatrix} + \begin{bmatrix} B_{1h} & B^{v-e}{}_{h-pos} \\ B_{2h} & B^{v-e}{}_{h-vel} \\ B^{h-e}{}_{v-pos} & B_{1v} \\ B^{h-e}{}_{v-vel} & B_{2v} \end{bmatrix} \begin{bmatrix} U_h(t) \\ U_v(t) \end{bmatrix} \tag{3.4}$$

$$y(t+1)=\begin{bmatrix}1 & 0 & 0 & 0\\ 0 & 0 & 1 & 0\end{bmatrix}\begin{bmatrix}pos_h(t+1)\\ vel_h(t+1)\\ pos_v(t+1)\\ vel_v(t+1)\end{bmatrix} \quad (3.5)$$

internal states of the model correspond to horizontal eye position (pos_h), horizontal eye velocity (vel_h), vertical eye position (pos_v) and vertical eye velocity (vel_v) (Equations 3.4 and 3.5). The state matrix, **A**, characterizes the influence of the current states on future states. Coefficients A_1-A_4 for the horizontal ($_h$) and vertical ($_v$) components (Equation 3.4; shaded blue) characterize the horizontal and vertical dynamics of the eye and were fixed from literature, with vertical dynamics equivalent to horizontal dynamics, to increase model tractability (Robinson et al., 1986). The input matrix, **B**, was used to weight the motor command to each state, where B_1-B_2 for both components were fixed to values obtained from the literature (Robinson et al., 1986). The remaining coefficients characterize interactions between horizontal and vertical position and velocity (Equation 3.4: shaded orange), where the superscripts *pos*, *vel* and *e* represent position, velocity and error along the associated direction. The inputs to the model were current horizontal and vertical eye positions, and the outputs were future horizontal and vertical positions.

The parameters for the state and input matrices derived from Robinson's time constants are shown in Equations 3.6 and 3.7 (Robinson et al., 1986). In this representation, there are no 2-D interactions between the horizontal and vertical states and parameters characterizing dynamics for the horizontal and vertical components are constrained to be equal to increase feasibility of model fitting (Chen-Harris et al., 2008).

$$A = \begin{bmatrix} A_{1h} & A_{2h} & 0 & 0 \\ A_{3h} & A_{4h} & 0 & 0 \\ 0 & 0 & A_{1v} & A_{2v} \\ 0 & 0 & A_{3v} & A_{4v} \end{bmatrix} = \begin{bmatrix} 0.9684 & 0.00898 & 0 & 0 \\ -3.0845 & 0.2374 & 0 & 0 \\ 0 & 0 & 0.9684 & 0.00898 \\ 0 & 0 & -3.0845 & 0.2374 \end{bmatrix} \quad (3.6)$$

$$B = \begin{bmatrix} B_{1h} & 0 \\ B_{2h} & 0 \\ 0 & B_{1v} \\ 0 & B_{2v} \end{bmatrix} = \begin{bmatrix} 0.0316 & 0 \\ 3.0845 & 0 \\ 0 & 0.0316 \\ 0 & 3.0845 \end{bmatrix} \quad (3.7)$$

Internal representations of the ocular dynamics and delays in response to corrective command signals are critical for accurate control in delayed feedback models. Here, accurate estimates of the plant and subsequent visual delay are incorporated into a Smith Predictor to reduce the error-inducing effects of feedback delays. Without this estimation, stable control systems operating on a dynamic error signal are limited to changes whose period is greater than the delay along the closed-loop path. With the forward model, the delayed visual feedback can be cancelled and replaced by a zero-lag estimate of the visual feedback, increasing the dynamic range of the system. To achieve the high accuracy in target tracking seen in healthy populations, the parameters characterizing the internal estimate of the ocular dynamics, $\widehat{A}$ and $\widehat{B}$ were set equal to the actual dynamics of the model (Equations 3.8 and 3.9).

$$A = \begin{bmatrix} A_{1h} & A_{2h} & A^{v-pos}{}_{h-pos} & A^{v-vel}{}_{h-pos} \\ A_{3h} & A_{4h} & A^{v-pos}{}_{h-vel} & A^{v-vel}{}_{h-vel} \\ A^{h-pos}{}_{v-pos} & A^{h-vel}{}_{v-pos} & A_{1v} & A_{2v} \\ A^{h-pos}{}_{v-vel} & A^{h-vel}{}_{v-vel} & A_{3v} & A_{4v} \end{bmatrix} = \begin{bmatrix} \hat{A}_{1h} & \hat{A}_{2h} & \hat{A}^{v-pos}_{h-pos} & \hat{A}^{v-vel}_{h-pos} \\ \hat{A}_{3h} & \hat{A}_{4h} & \hat{A}^{v-pos}_{h-vel} & \hat{A}^{v-vel}_{h-vel} \\ \hat{A}^{h-pos}_{v-pos} & \hat{A}^{h-vel}_{v-pos} & \hat{A}_{1v} & \hat{A}_{2v} \\ \hat{A}^{h-pos}_{v-vel} & \hat{A}^{h-vel}_{v-vel} & \hat{A}_{3v} & \hat{A}_{4v} \end{bmatrix} \quad (3.8)$$

$$B = \begin{bmatrix} B_{1h} & B^{v-e}{}_{h-pos} \\ B_{2h} & B^{v-e}{}_{h-vel} \\ B^{h-e}{}_{v-pos} & B_{1v} \\ B^{h-e}{}_{v-vel} & B_{2v} \end{bmatrix} = \begin{bmatrix} \hat{B}_{1h} & \hat{B}^{v-e}_{h-pos} \\ \hat{B}_{2h} & \hat{B}^{v-e}_{h-vel} \\ \hat{B}^{h-e}_{v-pos} & \hat{B}_{1v} \\ \hat{B}^{h-e}_{v-vel} & \hat{B}_{2v} \end{bmatrix} \quad (3.9)$$

The model of ocular dynamics reported by Robinson (Robinson et al., 1986) showed a position-dependent ocular drift that brings the eye back to center when fixating an eccentric position. This results in larger steady-state error between the eye and target as eccentricity increases, consistent with the known nonlinear viscoelasticity of the soft connective tissues involved in maintaining the eyeball in its orbit (Robinson, 1964, 1975; Westheimer, 1954). Figure 4 shows the response for the normative controller, in which steady-state error is dependent on position relative to visual axis. An ocular drift compensator gain on the target position was added to the saccade and smooth-pursuit control paths to negate the drift. Physiologically, this represents the constant torque applied to ocular muscles associated with fixation on an eccentric target. Manual tuning determined that a value of 1 was optimal for drift cancellation.

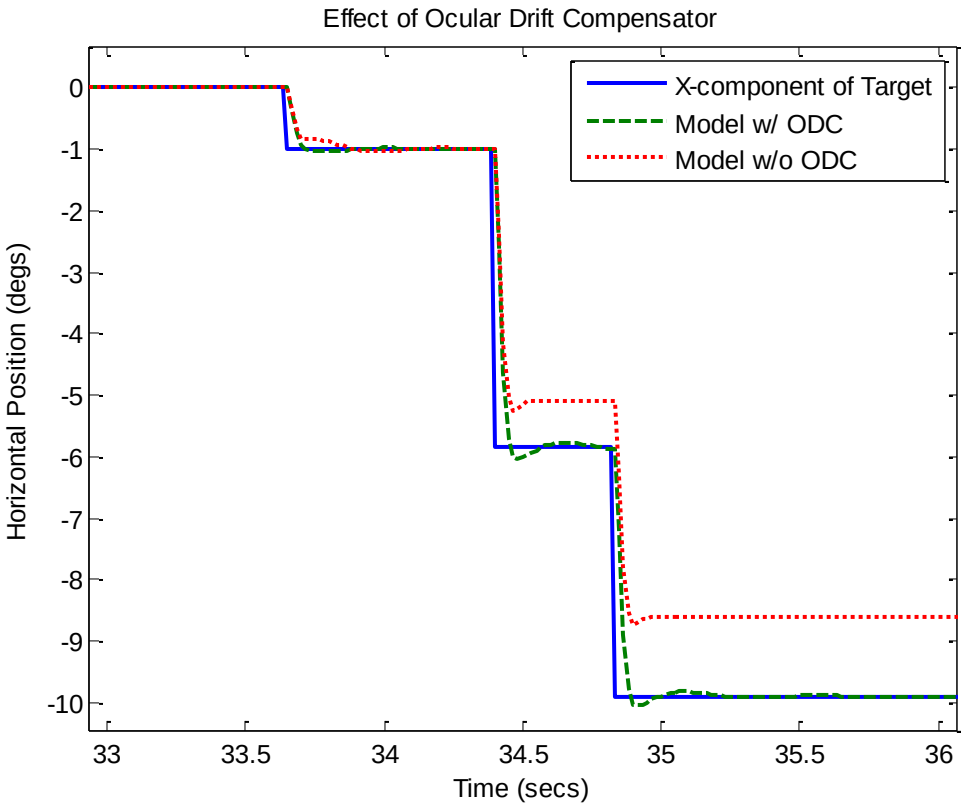

Figure 4: Model outputs showing the effect of drift compensation. Normative model without the ocular drift compensation (ODC; red dotted line) results in eccentricity-dependent steady-state error between the eye position and target that increases with eccentricity. Model with an ocular drift compensation gain of 1.0 (green dashed line), found through manual tuning, multiplied with the target amplitude to provide a constant torque needed to correct for ocular drift.

3.1.2 Saccade Loop

The saccade control loop acts as a discrete process that compensates for positional error greater than 0.5˚ (L. R. S. Young, L, 1963). The saccade motor command is driven by an extra-retinal error calculated between the eye and target positions. Saccade motor commands (U_h, U_v) are generated using a proportional-derivative (PD) controller (Equation 3.10) to drive changes in ocular position and velocity states using the

$$\begin{bmatrix} U_h \\ U_v \end{bmatrix} = \begin{bmatrix} P_h & D_h & 0 & 0 \\ 0 & 0 & P_v & D_v \end{bmatrix} \begin{bmatrix} Tpos_h - p\hat{o}s_h \\ \frac{d}{dt}\left(Tpos_h - p\hat{o}s_h\right) \\ Tpos_v - p\hat{o}s_v \\ \frac{d}{dt}\left(Tpos_v - p\hat{o}s_v\right) \end{bmatrix} \quad (3.10)$$

difference between horizontal and vertical target positions ($Tpos_h$ and $Tpos_v$) and perceived eye positions ($p\hat{o}s_h$ and $p\hat{o}s_v$) (Chen-Harris et al., 2008). For example, the model uses horizontal proportional (P_h) and derivative (D_h) gains with horizontal position error ($Tpos_h$ - $p\hat{o}s_h$) and velocity error ($^{d}/_{dt}$ ($Tpos_h$ - $p\hat{o}s_h$)) to compute the horizontal motor command. Interactions between horizontal and vertical motor commands were restricted to the state and input matrices. Prior to subject analysis, the controller gains were set to approximate the range of saccade velocities using model fits to averaged ballistic velocity profile and maximum velocity obtained from pilot data. During subject analysis, the controller parameters were fit to subject's saccade response to characterize motor generation using target position.

In the model, saccade commands were delayed before actuating the ocular plant. The delay was defined by a single lumped parameter that included propagation delays of the visual information and subsequent processing and generation of the saccade.

3.1.3 Smooth-pursuit Loop

Smooth-pursuit movements are slower than saccades and act to minimize steady-state tracking error, rather than merely bringing the eye to a region of interest. A proportional-integral-derivative (PID) controller was chosen as a general control mechanism to reduce both transient and steady-state error, where here, the proportional,

integrative and derivative gains modulate sensitivity to current error, accumulated error and the change in error, respectively. PID control has higher accuracy compared to PD control but requires a richer data set, as optimizing a larger number of parameters requires data with more distinct features. Equation 3.11 shows the smooth-pursuit motor command generation using position and velocity error. Horizontal and vertical motor commands are generated independently, indicated by zeros where axial (single axis) errors may influence cross-axial (opposite axis) motor commands.

$$\begin{bmatrix} U_h \\ U_v \end{bmatrix} = \begin{bmatrix} P_h(I_h+1) & D_h & 0 & 0 \\ 0 & 0 & P_v(I_v+1) & D_v \end{bmatrix} \begin{bmatrix} Tpos_h - p\hat{o}s_h \\ \frac{d}{dt}\left(Tpos_h - p\hat{o}s_h\right) \\ Tpos_v - p\hat{o}s_v \\ \frac{d}{dt}\left(Tpos_v - p\hat{o}s_v\right) \end{bmatrix} \quad (3.11)$$

Both the smooth-pursuit and saccade branches were similar in terms of the internal feedback path. Consistent with earlier smooth-pursuit eye movement models, the forward path uses a derivative function acting on the positional error to allow the system to operate on the change in error (velocity error) (Bahill & McDonald, 1983; Krauzlis & Lisberger, 1994; Robinson et al., 1986). Prior to the controller, the velocity error was rate limited to ±70 degrees/second to account for the shift from smooth-pursuit movements to saccades in response to high velocity targets (Bahill & McDonald, 1983).

3.2 Subjects

Nine healthy college students (4 Female; Mean age – 22.6 years, SD – 2.4 years) participated in the study. One of the nine subjects (EM_S02) was excluded from the

study due to persistent failure to track the visual target and reported ocular fatigue. Among the remaining subjects, three wore glasses regularly and one wore glasses occasionally. Although glasses were prohibited during the experiment, subjects verbally indicated they could identify target location on the screen. All subjects gave written informed consent prior to participation in accordance with Marquette University's Institutional Review Board.

3.3 Experimental Materials/Setup

The general setup used to experimentally measure eye movements is illustrated by Figure 5. An Arrington Research Systems BS007 Binocular EyeFrame Mounted EyeTracker® was used to track eye movements. The system uses two infrared (940nm) LEDs (one per eye) together with a pair of infrared CCD cameras to image the cornea of the subject's eye based on pupil roundness and corneal glint. Infrared (IR) corneal images are collected at 60 Hz with a USB-interface on a computer running Windows 7 and processed in real-time using Arrington Research's ViewPoint software system. The IR-LED sources are mounted on an eyeglass frame and placed approximately 2 cm from the eye. Prior to testing, the subject was fit with the head-mounted eyetracker and a head strap was used to prevent the eyetracker from slipping.

During a 1-hour test session, subjects participated in a series of eye movement tasks, in which they were asked to track the motion of a target (0.5˚ diameter) presented on a computer display. All tests were performed in the Integrative Neural Systems Lab, in a curtain-enclosed space to eliminate ambient lighting. Subjects were seated comfortably in a pivot-less chair 60 cm in front of a computer monitor and asked to place their head on a custom-made chin rest to minimize head movements during the task.

Figure 5: Experimental Setup (Wakde, 2011). The experimenter uses separate computers (left table) to generate stimuli and record eye movements. A chin rest positions the subject's head 60 cm in front of a NEC monitor. A switch box is used to direct displays at either a calibration grid from the eye movement data collection computer or stimuli from the computer running the experiment.

3.4 Visual Tasks

Stimuli were presented on a 41 x 30.5 cm NEC AccuSync 120 monitor with a 1400 x 1050 resolution at a refresh rate of 60 Hz, resulting in horizontal and vertical fields of view of 36˚ and 28˚ respectively. Stimulus generation and presentation was controlled using Bravishell and PsychToolbox 3.0.8 running in MATLAB R2010a (Mathworks, Natick, MA). Prior to testing, subject eye position was calibrated using an

Arrington (ViewPoint) 16-point calibration grid of sequentially displayed targets presented evenly spaced across the visual display.

Four visual tasks were used to quantify eye movements: saccade steps, smooth-pursuit ramps, combined saccade and smooth-pursuit targets and saccade threshold steps (the latter designed to characterize the target-response dead zone). Stimuli consisted of a target (yellow dot; 55 candela/meters square for both red and green colors) with a 0.5˚ diameter presented on a gray background (25 candela/meters square) that moved along the horizontal midline of the display, along the vertical midline of the display, and across the 2-D display, resulting in 12 task conditions. The direction of the target dot motion was randomized to minimize prediction of the target trajectory. For each task condition, 10 trials were obtained, each with a 10-second duration, to minimize the effects of fatigue (determined from a previous pilot study). No other features were present in the display. Thus, within the display, the only source of visual information was the target.

The duration, range of motion and types of sub-movements differed by task condition (described below). The target motion in each trial was generated randomly, reducing the chance of producing two trials with exact sub-movements.

3.4.1 Saccade Task

The random saccade task consisted of a visual target that performed a sequence of instantaneous displacements along the horizontal and/or vertical midline. The amplitudes of displacement were selected randomly from the range of 0-37˚, with the upper range corresponding to the full width of the display. The target was positioned at the display center at trial onset, and each new target location (T_N) was applied relative to the current target location (T_C), (Eq 3.10). Target locations were constrained to fall within the range

of the display. In each trial, the last displacement moved the target to the screen center for a minimum of 1 second to facilitate the concatenation of eye movement sequences across trials during analysis.

Following each random displacement, the target remained stationary for a pseudorandom interval ranging 0.0167-1.983 seconds. The duration range was used to characterize the amount of time required to fixate the target, and the pseudorandom selection of the displacement duration was used to prevent subjects from predicting the timing of eye movements. Subjects were instructed to move their eyes to the target as quickly and as accurately as possible.

3.4.2 Smooth-pursuit Task

During the smooth-pursuit task, the target moved in a series of constant velocity intervals along the horizontal and/or vertical midline with speeds ranging 1-20˚/seconds. At the start of each trial, the target was positioned at the center of display. The target then moved at a constant velocity in a randomly selected direction for period ranging 0.0167-3.983 seconds. The upper bound for the duration of movement was longer than that of the random saccade task to allow subjects sufficient time to match the velocity of the target. The target accelerated/decelerated at rates up to 15˚/seconds^2 for 75% of the movement intervals to reduce the predictability of the target movement. To minimize the occurrence of saccades between successive constant velocity/acceleration intervals, the new target location was momentarily equal to the previous target location such that the target followed a piece-wise continuous motion. When the target reached the bounds of the display, the target direction was reversed while maintaining the specified

speed/acceleration. During the last movement interval, the target moved at a predetermined speed of 18.43˚/seconds towards the display center. Given a maximum display half-width of 18.43˚, this ensured that the target reached the display center within the one second duration of the last interval. When the target reached the center, it remained stationary until the end of the trial to characterize gaze fixation. All trials began and ended at the display center to facilitate the concatenation of eye movements into a single time series to be fit by the model.

3.4.3 Combined Saccade and Smooth-pursuit Task

During each trial, the target followed a sequence of random displacements (saccades) and constant velocity/acceleration intervals (smooth-pursuit), similar to those described in the preceding tasks. The order of sub-movements was selected randomly and the duration of each sub-movement was randomly selected from the range 0.0167-1.983 seconds. Similar to the preceding tasks, the target was positioned at the center of the display prior to the first sub-movement and was returned to the center of the display during the last sub-movement interval. Smooth-pursuit target sub-movements had an arbitrary probability of three times that of saccade sub-movements due to the occurrence of catch-up saccades during smooth-pursuit movements.

3.4.4 Saccade Threshold Task

The saccade threshold task consisted of a series of target steps with amplitudes randomly selected from the range 0-2˚. The duration of each target step was randomly selected over the range 0.5-1.983 seconds, to allow subjects sufficient time to fixate the target. The target was positioned at the display center at trial onset and was displaced along the horizontal or vertical midlines, or across the 2-D display. In each trial, the last displacement moved the target to the screen center for a minimum of 1 second to facilitate the concatenation of eye movement sequences across trials.

3.5 Data Analysis

3.5.1 Data Preprocessing

Eye movement data collected from the eye tracker was pre-processed prior to the model fit to remove eye blinks using a pupil roundness algorithm (Eq. 3.10). Data points in which the pupil height to width ratio fell below 0.8 were removed and the remaining data were concatenated.

To align subject gaze data to the appropriate sub-targets, the eye tracking data during each 10-second trial was extracted using stimulus markers sent from Bravishell to the ViewPoint software to label the start and end points of each trial. Trials containing gaze artifacts (e.g. subject re-fixation during the task, in which subjects momentarily brought the eye position towards the screen center), were excluded from analysis. The remaining trials (≥5 per condition) were then concatenated to form a single continuous data set to aid model fitting.

To correct for slight head movements between trials, an amplitude offset was applied to each trial of the subject gaze data. This offset was computed as the difference between the mean positions (degs) of the target and subject gaze data. After subject gaze offset was corrected, the data was smoothed to reduce noise using a 100 ms sliding window. A gaze displacement threshold corresponding to 50% of the stimulus displacement was used to determine which targets displacements elicited a saccade. The gaze displacements were computed as the difference in positions across 133 ms durations, which were approximated as the durations of each saccade for the 2˚ displacement range from the saccade threshold task, to measure the full distance of a saccade displacement. To find the corresponding sub-target for every gaze point, the algorithm iteratively searched backwards in time for a unique non-zero sub-target displacement.

3.5.2 Initial-Model

Accurate fitting of the model to the eye tracking data required initial estimates for the model parameters that resulted in a stable system response, (see section 3.5.3 for more details). Initial conditions for the saccade's PD and smooth-pursuit's PID controllers were determined through a combination of inspection and model fitting to pilot data. The initial state for the model controllers was obtained by manually fitting the saccade and smooth-pursuit models to one randomly-selected (10-second duration) trial from the saccade and smooth-pursuit tasks obtained from two subjects in a separate pilot study. For the saccade task, the PD controller gains were adjusted until the rise time and overshoot error percentages were less that 10% between the two subjects. To capture the oscillatory movement about the dynamic target and low latency in the smooth-pursuit

data, the PID controller was tuned until model output matched the oscillatory motion seen at target onset of the data from one pilot subject (Figure 6). The initial parameter values for the vertical controller were then matched to those of the horizontal controller.

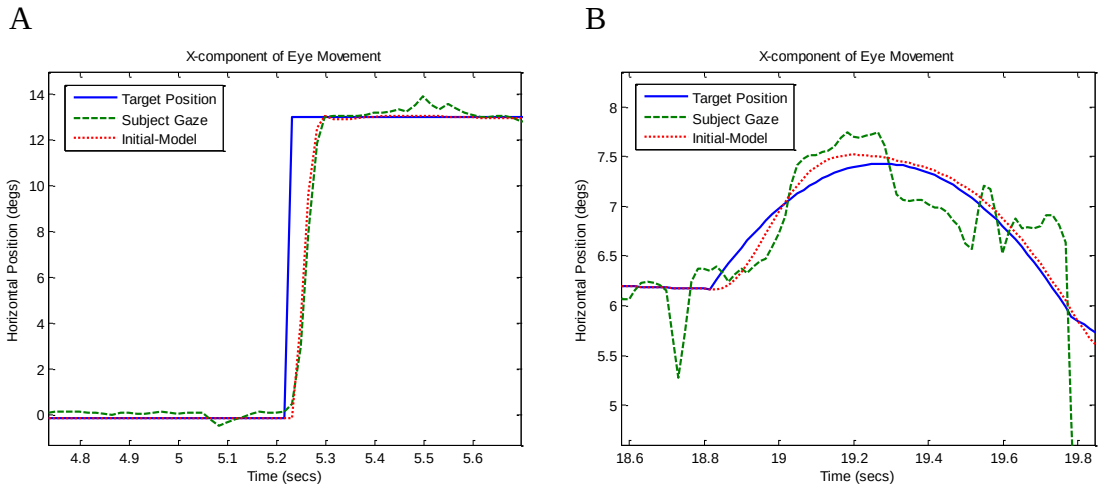

Figure 6: Saccade (A) and smooth-pursuit (B) controller outputs using the initial-model, compared to subject eye movements from pilot data. Saccade rise time error, calculated as the percent difference between the rise times of the target and subject step responses, was 8.108 %, and the saccade overshoot error, calculated as the percent difference between the overshoot values, was 9.491 %. The rise time and overshoot criteria were met for the saccade controller output, and the smooth-pursuit controller showed overshoot similar to subject data.

To further validate the initial-model controllers' tune to the pilot data, the model response characteristics were also compared to the literature. Two phenomena, the saccade main sequence (peak velocity as a function of displacement amplitude) and the smooth-pursuit main sequence (peak acceleration as a function of retinal slip velocity error), were evaluated for the model. Physiologically, both sequences show primarily a linear relationship, with velocity saturation shown in higher target amplitudes for saccades (Figure 7A,B). The exact saturation region varies across studies due to differences in data collection and differentiation techniques (Boghen *et al*, 1974). Figure 7 shows saccade and smooth-pursuit main sequences from earlier studies (A and B),

together with pilot data from one subject (C and D) and the model response (E and F). For the typical range of displacements used in the current study (<25 degs), the pilot data showed little (if any) saturation, making direct experimental estimation of the saturation point problematic. Figure 7 shows that the peak velocities from the saccade data in the literature and pilot subjects (A and C) show the same linear relationship (for displacements < 22 degs), with the pilot subjects showing peak velocities approximately half of those from the literature, likely due to a difference in eye tracker temporal resolutions between the studies affecting the accuracy of peak velocity computations with lower resolution here. The peak accelerations from the smooth-pursuit data in the literature and pilot subjects (B and D) resemble similar linear relationships, with the pilot subjects showing peak accelerations approximately an order of magnitude above those from literature. The lower peak accelerations from Lisberger's study may result from an attempt to remove catch-up saccades, which showed higher velocities than smooth-pursuit movements, through visual inspection of data (Lisberger et al., 1981). In the pilot data, the smooth-pursuit movements were smoothed by a 500 ms averaging window and assumed to contain no catch-up saccades.

Examination of the main sequence relationships suggested that saturation of the peak velocities and accelerations were not required in the model to represent the relationships from literature. Figure 7 shows that the peak velocities from the saccade data in pilot subjects and model (C and E) compare favorably in the linear region, but the pilot data does not consistently show peak velocities within a saturation region similar to the model. Similarly, without a peak acceleration saturation in the model, the peak

accelerations from the smooth-pursuit data compare favorably (D and F). Therefore the saturations of velocity and acceleration points were not implemented in the model.

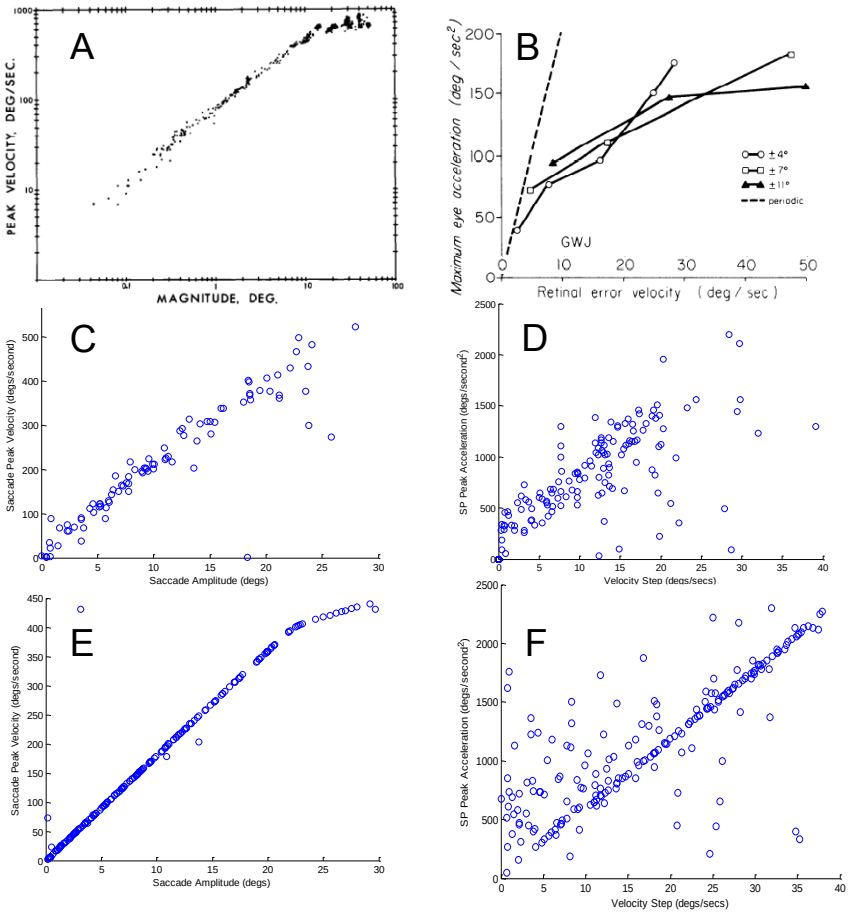

Figure 7: Main sequences for saccades and smooth-pursuit eye movements defined as the peak velocity to displacement during saccades, and peak acceleration to velocity for smooth pursuit. (A) and (B) show the main sequences for saccades (A. T. C. Bahill, M.R.; Stark, L, 1975) and smooth pursuit (Lisberger et al., 1981) from literature. The main sequence from the saccade sub-model with velocity saturation (E) approximates the linear and saturation regions of the main sequence of recorded eye movements from earlier studies (A) and the linear region of the pilot data (C). The main sequence from the smooth-pursuit sub-model (F) resembles the linear main sequence seen in earlier studies (B) and peak accelerations seen in the pilot data (D).

3.5.3 System Identification

Figure 8 shows the workflow for the 3-stage system identification process used to characterize the model parameters in response to subjects' responses to the oculomotor

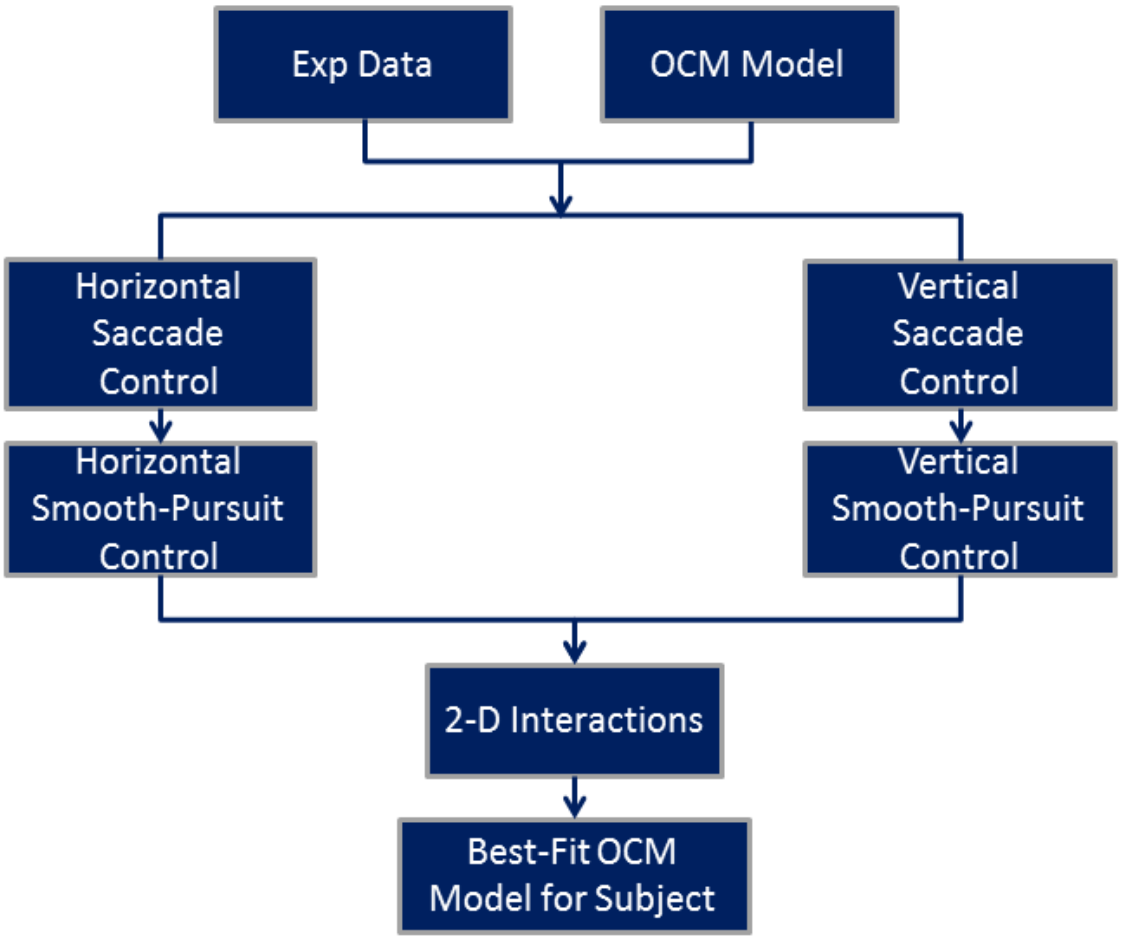

Figure 8: Workflow for System Identification Process. The experimental data and oculomotor control model were input to the predictive error minimization algorithm that yielded the best-fit parameters. Axial components of the same task types comprised the data used to acquire parameters for saccade, smooth-pursuit and 2-D control. The end result of this workflow is the subject-specific best-fit oculomotor control model.

tasks. The structure and free parameters of the oculomotor model were defined using the nonlinear greybox identification object (idnlgrey) in the Systems Identification Toolbox (Matlab, 2012). The predictive error minimization (PEM) function was used to optimize the free parameters by minimizing a least squared error cost function. The PEM function

simultaneously and systematically adjusted all free parameters iteratively using the Gauss-Newton algorithm (Rovati, 1990). After each iteration, the updated model output was estimated from the new parameter estimates to determine if the model change contributed to a lower cost. Observations from model fitting to pilot data showed parameter estimates typically reached a steady-state within 10 iterations, so the PEM function was limited to 10 iterations before beginning a new fit. Using a minimum error bound that was a percentage of the cost function in real time required more simulation time (up to a factor of 20) to reach the error bound.

During the model fit, only the controller gains and 2-D interaction parameters were fit to the visual tracking tasks. Model parameters characterizing ocular dynamics, rate limiter and velocity saturation were fixed at average values obtained from the literature. The dead zone, saccade processing delay and smooth pursuit processing delay were calculated directly from eye movement responses during the tasks. The dead zone was measured from the saccade threshold task as the smallest sub-target displacement shown to induce a saccade response. Delays between target displacement and saccade onset were computed for each sub-target (10 per trial) in the random saccade tasks by detecting when subject's gaze moved 50% of the target displacement. These delays were averaged, with values beyond one standard deviation (optimized threshold verified with time-series of saccade data from pilot data) identified as errors in the saccade detection and removed. Delays associated with smooth-pursuit were measured from the smooth-pursuit tasks using cross-correlation between the target position and subject's gaze to identify the shift needed for maximum overlap.

Temporal mismatch between the target and subject eye movement compounds error in the parameter estimates from model fitting. To minimize this mismatch, the subject gaze data from each trial were backward-shifted in time using the trial-wise delay. Performing this shift on each trial accounted for the effect of inter-trial variability in delays.

At the beginning of each model fit, initial conditions were randomly selected from a range spanning two orders of magnitude centered on the base values (the initial model whose parameters were optimized to pilot data; see section 4.1.3 for additional details), to characterize the uncertainty in the model fits.

The model was fit to the experimental results in stages by task condition. During the first stage, the horizontal and vertical PD gains for the saccade controller were fit to the subject's eye movements from the horizontal and vertical saccade tasks, respectively. During the second stage, the horizontal and vertical PID gains for the smooth-pursuit controller were fit to the subject's eye movements from the horizontal and vertical smooth-pursuit tasks, respectively. For each PID fit, the controller gains in the saccade path were randomly drawn from the distribution of estimates obtained in the stage-one fits and held constant. This considerably expanded the parameter space for the smooth-pursuit controller fits to increase the probability of capturing more accurate combinations of parameter estimates for the subject data, as shown in Figure 9. For example, during

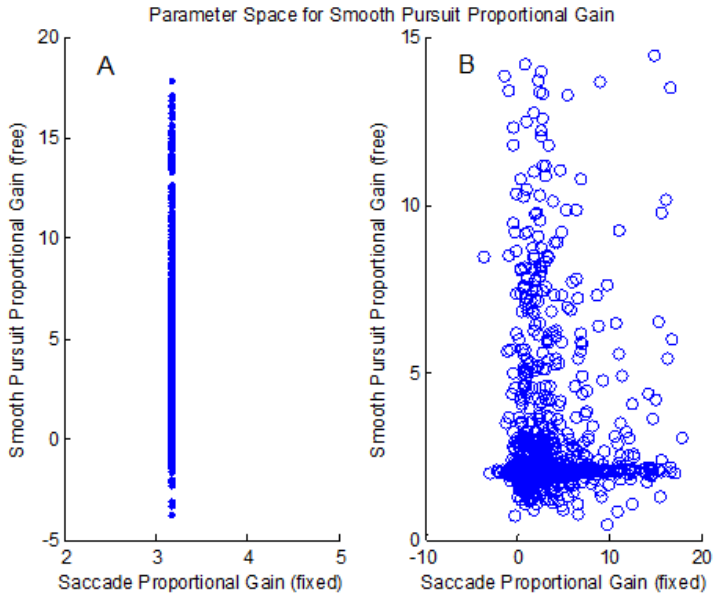

Figure 9: Parameter Space for 2nd stage fitting to a single parameter. Each circle corresponds to final estimates of a model fit. A) Effect of using the average saccade proportional gain from stage 1 on the range of final estimates obtained for smooth pursuit proportional gain obtained from the second stage fit. B) Effect of randomly selecting a constant saccade proportional gain from the distribution of estimates in the stage 1 fit on the range of final estimates obtained for smooth pursuit proportional gain obtained from the second stage fit. Subplot B shows initial conditions for the saccade proportional gain expanding a greater range of values, which is intended to increase the probability of the model finding the optimal combination of parameters to fit to the subject data. Note that the L-shape resulting from clustered points indicates a skewed distribution for both parameters.

fits of the horizontal smooth-pursuit controller gains, horizontal saccade controller gain pairs were randomly selected from the stage-1 fits and held constant during the smooth pursuit fit. During the third stage, the interactions between horizontal and vertical movements characterized by the 2-D ocular dynamics (state matrix) and motor command weights (input matrix) were fit to subjects' responses from the 2-D tasks. During the stage three fits, the 1D saccade and smooth pursuit control parameters were randomly sampled from the stage 1 and 2 distributions and held constant. The interaction parameters were fit to the 2-D saccade and smooth-pursuit trials separately to quantify the effects of task on these parameters. Two sets of interaction parameters correspond to the saccade and smooth-pursuit tasks and are presented separately.

3.5.4 Bootstrap Analysis

To characterize the distribution of best-fit parameters, a bootstrap analysis of at least 1000 model fits was performed for each subject and at each stage of the model fit. This is a systematic approach to quantify the uncertainty of the estimates.

To remove parameter estimates corresponding to unsuccessful fits, such as insensitive fits where the initial conditions are returned or unstable fits where the parameter estimates elicit an unstable response, three computational filters were used. The first filter removed model fits where the best-fit parameters were equal to initial conditions. The second filter removed inaccurate fits that included any horizontal and vertical positional errors that were greater than 10% of the screen width and height respectively. The third filter removed fits whose best-fit parameters were five standard deviations from the average best-fit parameter value.

Parameter estimates characterized by a normal distribution can be reported as the mean and standard deviations across the bootstrap distribution (or trial-wise estimates) to facilitate statistical analyses within and across subjects. Distributions for all parameters in this study showed some degree of skewness (approximately -1 to 2.5) and were first transformed to a normal distribution using a box-cox transformation, (Equation 3.13).

$$trans(data) = \frac{data^{\lambda} - 1}{\lambda} \qquad (3.13)$$

The transformation parameter (lambda) was determined using the boxcox function in Matlab to maximize the log-likelihood function of the transformed data to a normal

distribution. The transformed data tended to be shifted from the original data as a side effect of the transformation. To facilitate comparisons in conventional units, the mean value of the transformed distribution was inverse-transformed using Equation 3.14.

$$mean = \left\{(\lambda)\times\left(mean\left[trans\left(data\right)\right]\right)+1\right\}^{1/\lambda} \qquad (3.14)$$

Since the box-cox transformation requires positive values, data sets were shifted prior to the transform by the minimum value needed to bring all values to the positive range prior to transformation. Thus, parameters yielding negative values required a post-shift of the inversed-transformed mean (Equation 3.15). The 95% confidence interval, using 2

$$mean = \left\{(\lambda)\times\left(mean\left[trans\left(data\right)\right]\right)+1\right\}^{1/\lambda} + shift \qquad (3.15)$$

standard deviations, was obtained from the transformed distribution using Equations 3.16 and 3.17, where CI (5%) and CI(95%) are the values for the lower and upper bounds of the 95% confidence intervals, respectively.

$$CI(5\%) = \left\{(\lambda)\times\left(mean(data) - 2\times std\left[trans\left(data\right)\right]\right)+1\right\}^{1/\lambda} + shift \quad (3.16)$$

$$CI(95\%) = \left\{(\lambda)\times\left(mean(data) + 2\times std\left[trans\left(data\right)\right]\right)+1\right\}^{1/\lambda} + shift \quad (3.17)$$

In cases where the boot-strap distribution was bimodal (~20% of fitted parameters), a double-Gaussian fit was applied to the bimodal box-cox transformed

distribution of each parameter using the Levenberg-Marquardt algorithm to minimize the least squares error. The distance between the two estimated means, normalized to the 95% confidence intervals of the two distributions, was compared to a threshold of 0.75 (optimized to EM_S01's estimated saccade and smooth-pursuit controller gains that showed bimodal distributions) to automatically flag bimodal distributions. A threshold value of 1.0 corresponds to the upper 95% of one primary distribution overlapping with the lower 5% of the distribution. The distance between distributions revealed the degree of distinction between parameter estimates, and the relative width of the distributions was characterized by the amount of overlap. Equation 3.18 summarizes this approach, where B is the binary-encoded flag, μ is the mean, σ is the 95% confidence interval and α is the optimized threshold. Bimodal distributions flagged during the bootstrap analysis were manually inspected to determine if the flag was accurate and whether one or both means were used to represent a parameter for a given subject; with two estimates likely suggesting two control modes for the given task.

$$B = \begin{cases} 1 & if \quad (\mu_1 - \mu_2) > \alpha\left(avg(\sigma_1, \sigma_2)\right) \\ 0 & if \quad (\mu_1 - \mu_2) < \alpha\left(avg(\sigma_1, \sigma_2)\right) \end{cases} \tag{3.18}$$

4 RESULTS

4.1 Analyses Prior to Model Fitting

4.1.1 Delay Analysis

Figure 10 shows the measured oculomotor delays for saccades and smooth pursuit eye movements. Across subjects, the average latencies for saccades and smooth-pursuit eye movements were 242 (± 24) ms and 107 (± 33) ms, respectively (Figure 11). This is comparable to saccade latencies of 200 ms smooth-pursuit latencies of 100 ms reported in earlier studies (Erkelens, 2006; Meyer et al., 1985; Orban de Xivry & Lefevre, 2007). Paired t-tests of saccade ($t(8)=-0.82$, $p=0.42$) and smooth-pursuit ($t(8)=0.42$, $p=0.68$) showed no significant difference between horizontal and vertical latencies across subjects.

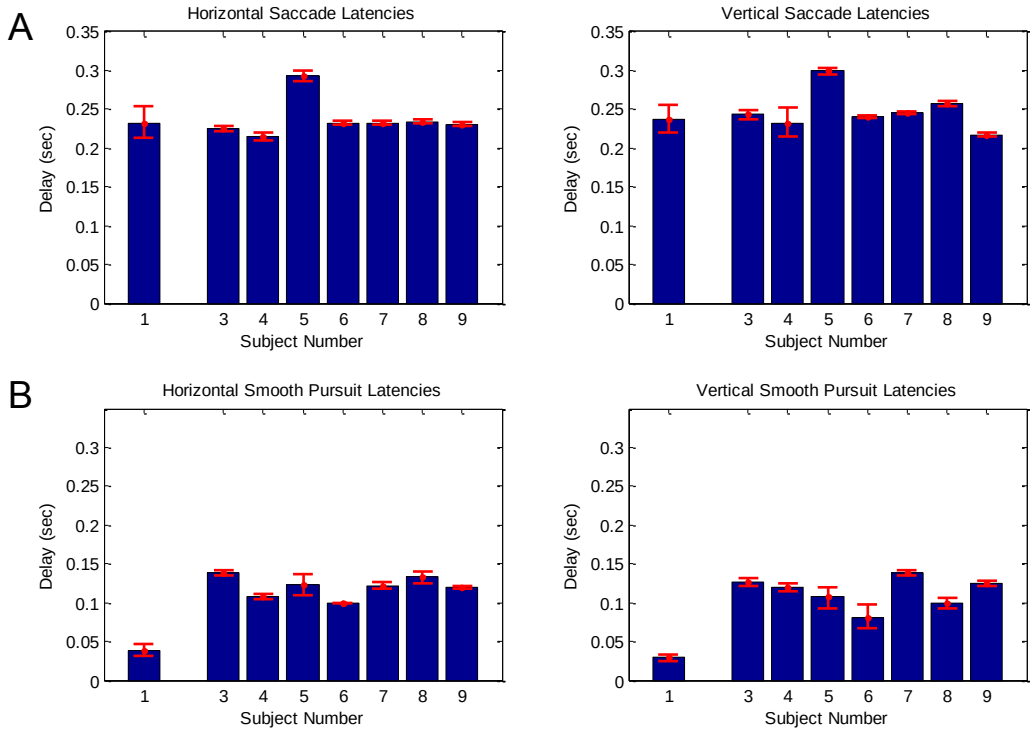

Figure 10: Average saccade and smooth-pursuit latencies across trials (±1 S.E.) for horizontal and vertical (A) saccades and (B) smooth-pursuit eye movements.

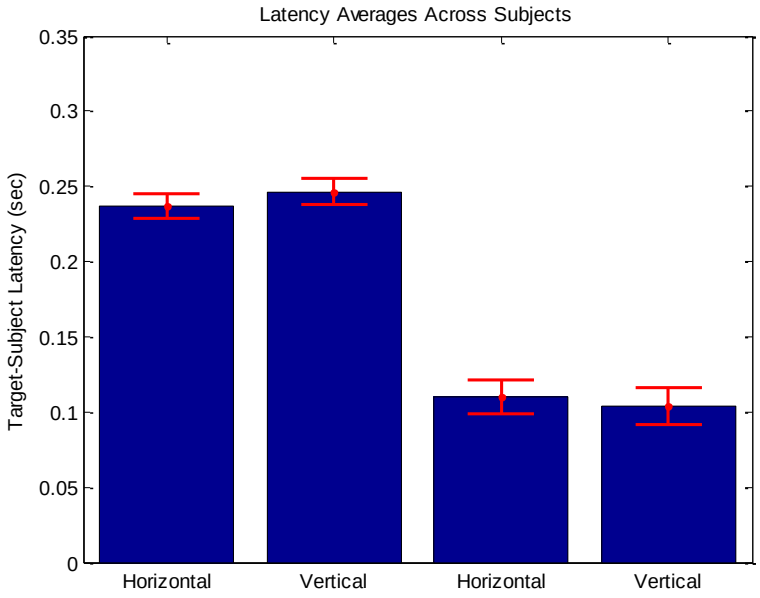

Figure 11: Task-dependent latencies averaged across all subjects. Error bars denote ± 1 S.E. about the mean.

4.1.2 Dead Zone Analysis

The dead zone places a lower threshold on the eye position error required to enable the saccade controller. Analysis of the saccade threshold task was used to determine displacement needed to initiate a corrective saccade for each primary saccade (see Section 3.4.4).

Two metrics were used to determine the position error threshold for saccade onset: saccade percentage (percentage of detected saccades for a given number of sub-targets) and component-wise dead zone (minimum saccade displacement detected). The percentages of sub-targets eliciting a saccade averaged across all subjects were 96.67 (±3.14) % and 93.51 (±5.02) % for the horizontal and vertical components, respectively. The average dead zones across all subjects, determined as the minimum stimulus displacement to elicit a saccade, were 0.027 (±0.034)˚ and 0.0133 (±0.009)˚ for horizontal and vertical displacements respectively. Both values are more than one order of magnitude less than the reported dead zone of 0.5˚, required to illicit a saccade-response (L. R. S. Young, L, 1963), suggesting an inability of the mode/measurement system to accurately characterize the dead zone. The dead zone values in this study could be affected by the reported 0.5˚ accuracy of the eye tracker (Arrington), and the measured eye displacements below 0.5˚ may be residual noise resulting from an ineffective smoothing window of 100 ms. In addition, the saccade threshold task had a 0-2˚ sub-target displacement range in which very small sub-target displacements identified small eye displacements as saccades. For example, Figure 12 A showed that all small sub-target displacements (<0.5˚) had eye displacements that were within 50% of the sub-target displacement, and Figure 12 B appropriately showed sub-target displacements

under 0.5˚ all elicited saccades. For the subsequent parametric analysis, saccade thresholds were set to the literature value of 0.5˚ to provide a general characterization of the transition between smooth pursuit and saccade control.

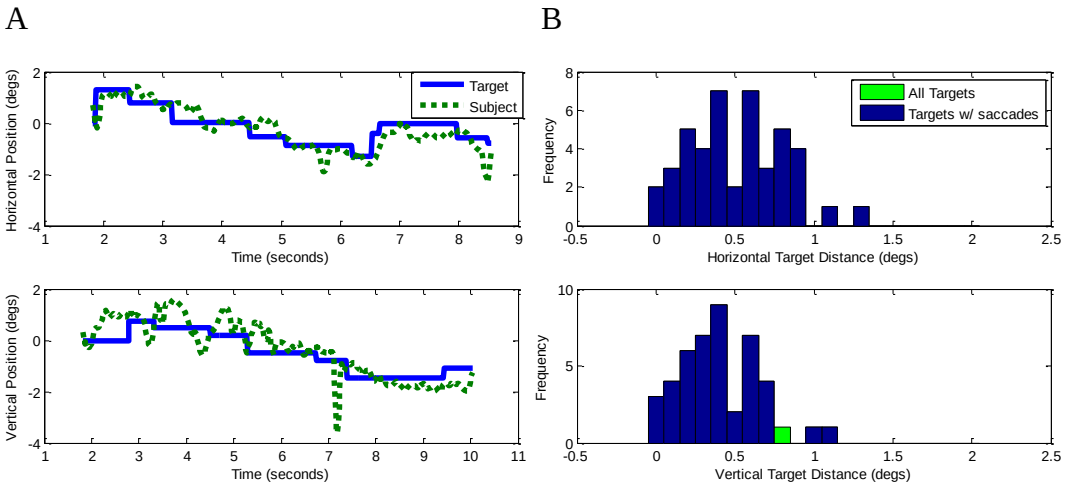

Figure 12: (A) Example time-series from a typical subject (EM_S03). The limited resolution of the eye tracker (~0.5 deg) likely contributed to the variation in subject's eye movement (dashed line) about the target position (solid line). (B) Example histogram of target sub-movements eliciting saccades from a typical subject (EM_S03). Nearly all target sub-movements showed corresponding saccades (the green bar shows the only target sub-movement without a corresponding saccade). As seen here, target sub-movement displacements as small as 0.0133 degrees produced saccades.

Subject	Horizontal Saccade Percent	Vertical Saccade Percent	Horizontal Threshold (degs)	Vertical Threshold (degs)
1	93.33	88.89	0.03	0.03
3	100.00	97.78	1e-03	0.01
4	91.11	88.37	0.07	0.02
5	97.78	95.24	2.6e-03	0.02
6	97.78	86.67	0.01	0.01
7	95.56	93.33	3.4e-03	2.5e-03
8	97.78	97.78	0.01	0.01
9	100.00	100.00	0.09	0.01

Table 1: Dead zone estimates for each subject. The horizontal and vertical saccade percentages indicate the number of detected saccades per sub-target displacement. The threshold values indicate the minimum sub-target displacement needed to elicit a saccade.

4.1.4 Accuracy and Precision Analysis

Prior to fitting the model to subject's eye movement data, the accuracy and precision of fitting the model parameters to task-specific eye movements was characterized. This provided an estimate of the bias and uncertainty in parameter estimates relative to known values drawn randomly from the range of initial conditions (ICs). A -10 to 10 factor range of the true value was used as the perturbation, or IC, range.

A model with known parameter values was used to generate simulated data sets that were subsequently fit by an unconstrained model with randomly sampled ICs. Parameters including the 1-D ocular dynamics (plant) and dead zone were fixed to values from literature and were not perturbed during this analysis. Free parameters, including the 1-D controller gains and 2-D system interactions, were fixed to values from the initial-model (nominal values) and were individually perturbed one-at-a-time. The 2D interaction parameters, $A^{\text{v-pos}}{}_{\text{h-vel}}$, $A^{\text{h-pos}}{}_{\text{v-vel}}$ and $B^{\text{v-e}}{}_{\text{h-vel}}$ were fixed to 0.3, 0.2 and 0.1 respectively. The remaining 2-D interaction parameters were fixed to 0.01 based on fits to pilot data. To evaluate the accuracy and precision of fitting each parameter, 1000 model fits were made to 50 seconds of simulated eye movements. A box-cox transformation was then applied (Equations 3.13 and 3.14) to normalize the distributions and estimate the best-fit parameter.

The accuracy of the model fits was evaluated by comparing the nominal values with the best-fit values from the bootstrap analysis. The relative standard deviation as a percentage of the mean (best-fit) value was computed from the box-cox transformed distributions using Equation 4.2 (PNNL, 2008) to evaluate the precision of the model fit

for each parameter. The 95% confidence interval was used to characterize the skewness in the distribution and the z-score (Equation 4.3) was used to quantify the accuracy of the best-fit estimate relative to the nominal value.

$$\text{RSTD\%} = \frac{\text{Standard Deviation}}{\text{Best-Fit Estimate}} \times 100 \qquad (4.2)$$

$$\text{Z-score} = \frac{|\text{Best-Fit Estimate - Nominal}|}{\text{Standard Deviation}} \qquad (4.3)$$

. Parameter	Nominal	Estimated	RSTD%	95% Conf Int	Z-score
Saccade P gain	3.76	3.73	1.61	3.54-3.82	0.517
Saccade D gain	0.0418	0.0417	0.17	0.0416-0.0419	0.911
SP P gain	1.75	0.55	519.1	-8.07-5.12	0.4163
SP I gain	0.75	0.73	7.79	0.58-0.82	0.337
SP D gain	0.02	-0.0041	106.9	-0.017-0.003	5.466
$A^{\text{v-pos}}_{\text{h-pos}}$	0.01	0.007	285.8	-0.038-0.043	0.156
$A^{\text{v-vel}}_{\text{h-pos}}$	0.01	0.007	90.6	-0.009-0.017	0.513
$A^{\text{v-pos}}_{\text{h-vel}}$	0.3	0.34	213.3	-1.375-1.644	0.057
$A^{\text{v-vel}}_{\text{h-vel}}$	0.01	0.013	165.3	-0.033-0.051	0.121
$A^{\text{h-pos}}_{\text{v-pos}}$	0.01	0.006	267.8	-0.038-0.006	0.303
$A^{\text{h-vel}}_{\text{v-pos}}$	0.01	0.007	69.7	-0.007-0.015	0.635
$A^{\text{h-pos}}_{\text{v-vel}}$	0.2	0.22	193.9	-0.926-0.946	0.052
$A^{\text{h-vel}}_{\text{v-vel}}$	0.01	0.012	185.5	-0.041-0.050	0.082
$B^{\text{v-e}}_{\text{h-pos}}$	0.01	0.006	444.6	-0.046-0.017	0.145
$B^{\text{v-e}}_{\text{h-vel}}$	0.1	0.094	179.9	-0.275-0.426	0.021
$B^{\text{h-e}}_{\text{v-pos}}$	0.01	0.009	262.2	-0.031-0.062	0.045
$B^{\text{h-e}}_{\text{v-vel}}$	0.01	0.014	46.7	0.003-0.028	0.567

Table 2: Sensitivity analysis results for the controller and 2-D interaction parameters using initial-model values. The nominal values of the parameters are compared with the best-fit estimates obtained from a bootstrap analysis of 1000 fits. Estimation certainty and skewness are characterized by the 95% confidence intervals in parameter estimates from the box-cox distributions. The relative standard deviation percentage (RSTD%) was used to quantify the precision of parameter estimation. The box-cox transformed mean and standard deviation values from the parameter distributions were used to compute the z-score that quantifies the difference between the best-fit and nominal values of the parameter in units of standard deviations. Sixteen of the 17 best-fit parameter estimates were

within one standard deviation from the nominal value. The estimate for the smooth-pursuit integral gain (SP I gain) was more than 5 standard deviations from the nominal value, suggesting that the parameter estimate was inaccurate and may be unreliable for fitting to subject data.

The controller parameters were generally precise with the exception of the proportional and derivative gains of smooth-pursuit control. The lack of precision suggests these parameters are less sensitive to changes in the model that lower the positional error, resulting in a wide range of estimates. This could suggest that the values of the initial-model, around which the initial parameter estimates are sampled, and the ranges/types of motion tested may not have adequately spanned the space needed to properly fit the integral gain.

The parameters characterizing the interactions between horizontal and vertical eye movements had less precision than the saccade and smooth-pursuit control parameters. Interestingly, the velocity-on-position effect for both directions had standard deviations within 100% of the best-fit estimate. The horizontal error's influence on the vertical velocity had the most precision: one standard deviation within 46.7% of the best-fit estimate. One explanation for differences in precision between horizontally-based parameters ($A^{\text{h-pos}}_{\text{v-pos}}$, $B^{\text{h-e}}_{\text{v-vel}}$…etc.) and vertically-based parameters ($A^{\text{v-pos}}_{\text{h-pos}}$, $B^{\text{v-e}}_{\text{h-vel}}$…etc.) is based on the randomly-chosen data set, where larger horizontal targets give more influence to horizontally-based parameters and *vice versa*.

The z-scores indicated that 16 of 17 parameters had best-fit values estimated within 1 standard deviation from their nominal values. The exception was the derivative gain of the smooth-pursuit control (z-score=5.466), which suggests that the estimation of this parameter is unreliable for our model. Its estimation to a negative value suggests a preference to add resistance to the smooth-pursuit movement already initiated by the

fixed proportional and integral gains, which points to a flaw in the initial-model development where individual parameter performance was not evaluated thoroughly enough. The best-fit estimation of the derivative gain suggests that a more optimal initial-model would hold a negative derivative gain. A negative derivative gain negating the effect of the proportional and integral gains seems counter-intuitive. Once again, it should be noted that the ranges/types of motion tested may have inadequately allowed the model to accurately find a positive derivative gain.

4.2 Parametric Analysis

4.2.1 Saccade Controllers

Fitting the saccade sub-model to the time-series of the random saccade task yielded average R^2 values of 0.964 and 0.947 across subjects for the horizontal and vertical components, respectively. An example time-series of subject and model gaze is shown in Figure 13 and Figure 14.

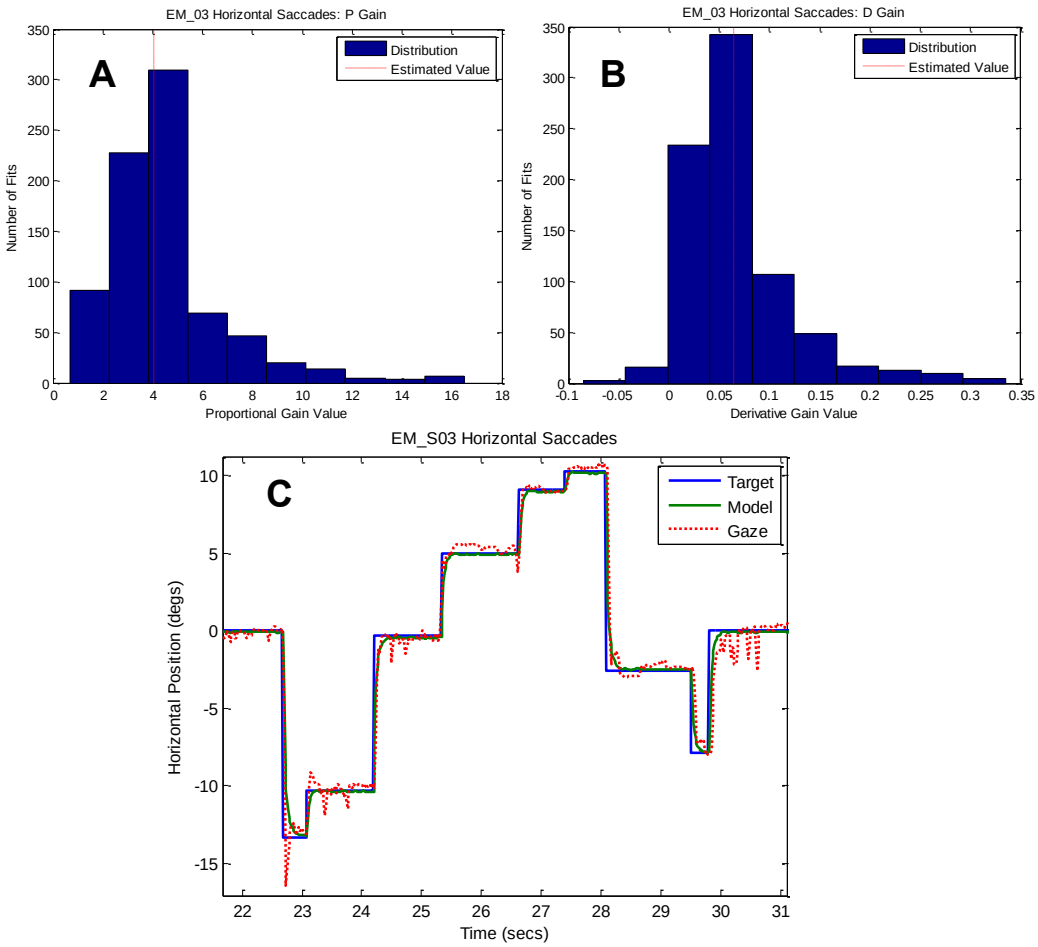

Figure 13: Sample Fit to the Horizontal Saccade Task for (EM_S03). The saccade latencies from the subject data were minimized using cross-correlation. Distributions of the best-fit estimates for the (A) proportional gain and (B) derivative gain of the saccade controller across 1,000 fits. The red dashed line shows the median of the distribution. The horizontal proportional and integral gains were estimated as 4.01 and 0.062, respectively. C) Time-series of one trial for subject 3 used to estimate the horizontal controller parameters. The R^2 value of the best-fit response based on the parameter estimates was 0.9773 across all horizontal saccade trials.

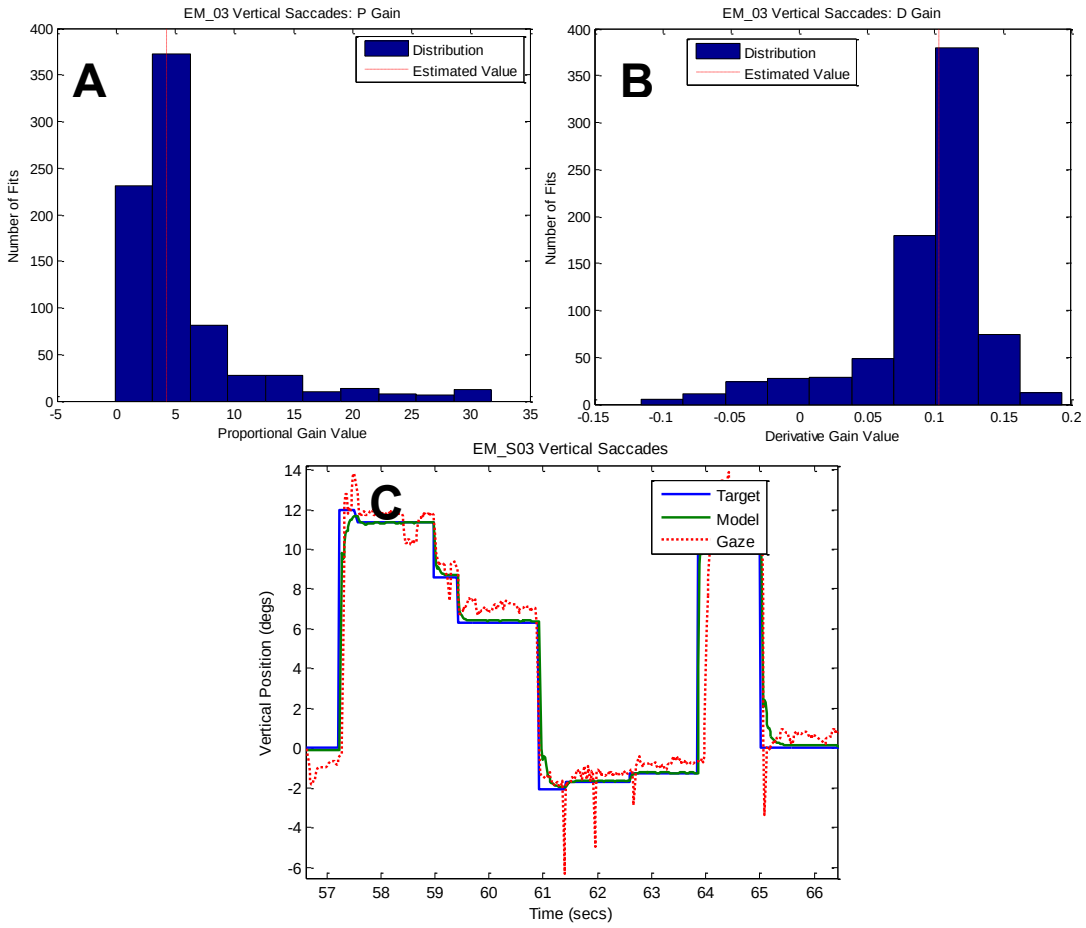

Figure 14: Sample Fit to the Vertical Saccade Task for Subject 3. Distributions of the best-fit estimates for the (A) proportional gain and (B) derivative gain of the saccade controller across 1,000 fits. The red dashed line shows the median of the distribution. The vertical proportional and integral gains were estimated as 4.31 and 0.1, respectively. C) Time-series of one trial for subject 3 used to estimate the vertical controller parameters. The R^2 value of the best-fit response based on the parameter estimates was 0.9287 across all vertical saccade trials.

The horizontal and vertical saccade controllers were characterized separately, with horizontal controller parameters fixed when fit to vertical saccades, and *vice versa*. Both the proportional and derivative gains tended to show higher values in the vertical direction than in the horizontal direction (Figure 15), however, the difference was not statistically significant (proportional gain: t(14.09)=-0.96, p=0.35; derivative gain: t(13.06)=-0.24, p=0.81).

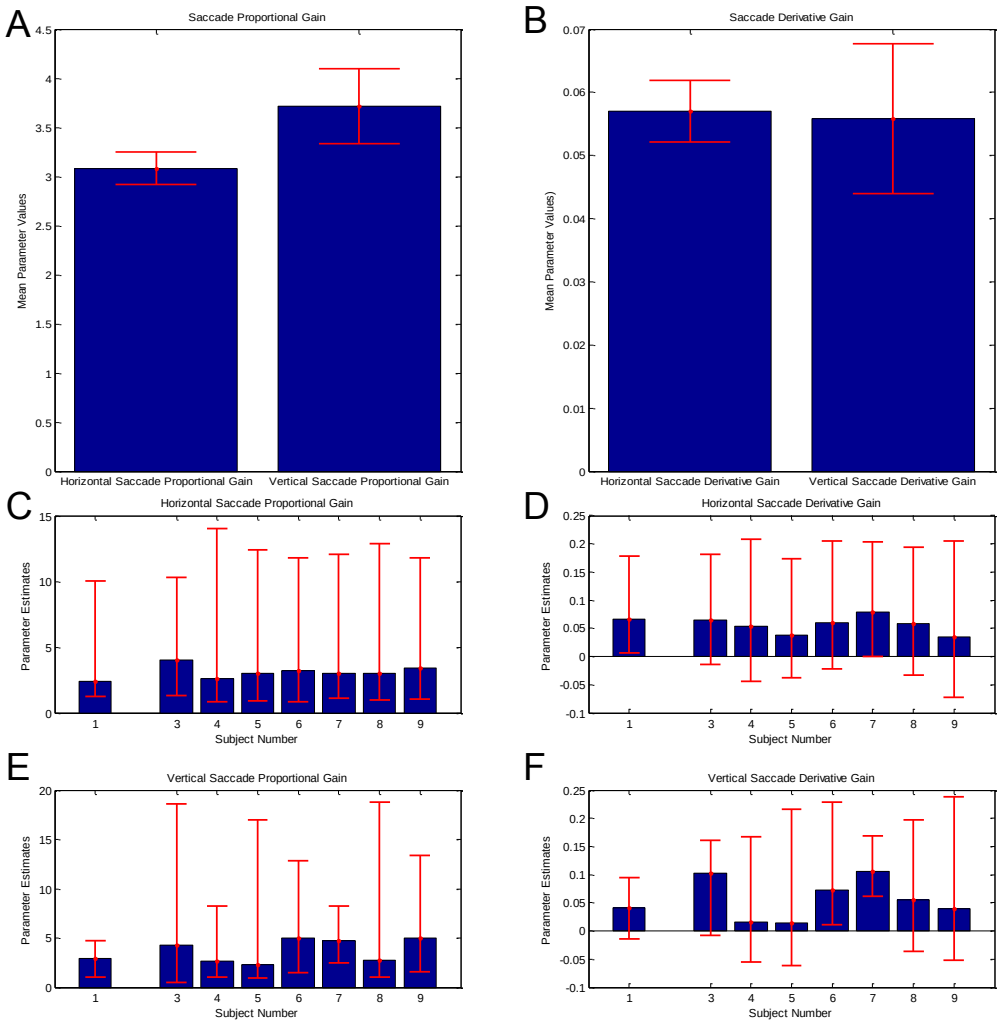

Figure 15: Box-coxed transformed mean of saccade controller gains across subjects. The average parameter estimates across subjects for the proportional (A) and derivative (B) gains of the saccade controller are shown (± 1 SE). Individual estimates of the proportional and derivative gains are shown in (C) and (D). Likewise, the vertical saccade task was used to estimate the vertical proportional (E) and derivative (F) gains. Solid red lines denote the 95% confidence interval. The distribution mean for each subject's was obtained from 1000 separate model fits and all showing R^2 values > 0.91 between the subject data and best-fit model's response. Note that subject 2 was excluded from all analysis.

4.2.2 Smooth-pursuit Controllers

The proportional, integral and derivative gains for the smooth-pursuit controller were fit simultaneously for horizontal and then the vertical eye movements. Unlike

fitting to the saccade controller, where the base values were fixed to the initial-value model, the smooth-pursuit controller was coupled with fixed values of the saccade controller drawn from their respective bootstrap distributions obtained from the saccade task. Figure 16 and Figure 17 show the distributions and sample time-series for subject EM_S03 for the horizontal and vertical smooth pursuit eye movements, respectively. In subject EM_S03 and most subjects, the distribution of best-fit gains for the horizontal and vertical smooth-pursuit controllers, show considerable right skewness. The skewness is driven in part by the need to have positive integral gains to reduce visual tracking error. It should be noted that the model shows very few catch-up saccades. This may reflect a strategic difference associated with the model fitting whereby an aggressive smooth-pursuit control, versus weak control aided by catch-up saccades, may better minimize error between the model and subject gaze data.

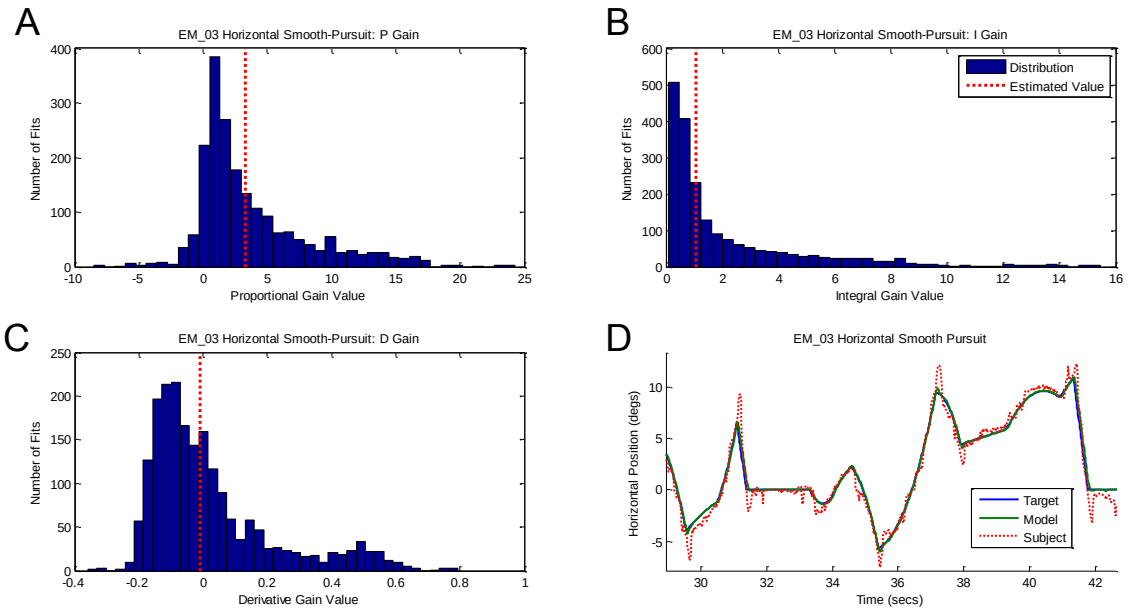

Figure 16: Sample fit to the Horizontal Smooth-Pursuit Task (EM_S03). Distributions for the proportional (A), integral (B) and derivative (C) gains for horizontal smooth-pursuit were fitted simultaneously while the vertical gains were held constant. Subject 3's proportional, integral and

derivative gains were estimated as 3.30, 1.08 and -0.01, respectively. D) Example subset of visual tracking data used to fit horizontal smooth-pursuit control.

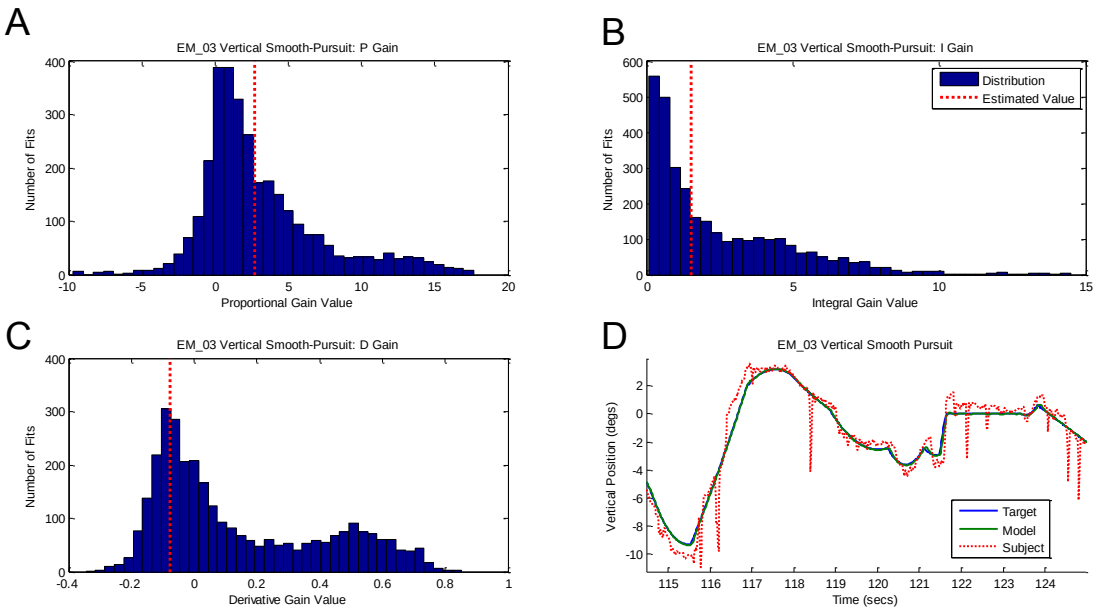

Figure 17: Sample Fit to Vertical Smooth-Pursuit Task (Subject 3). Distributions for the proportional (A), integral (B) and derivative (C) gains for vertical smooth-pursuit were fitted simultaneously while the horizontal gains were held constant. Subject 3's proportional, integral and derivative gains were estimated as 2.73, 1.52 and -0.08, respectively. D) Example subset of visual tracking data used to fit vertical smooth-pursuit control.

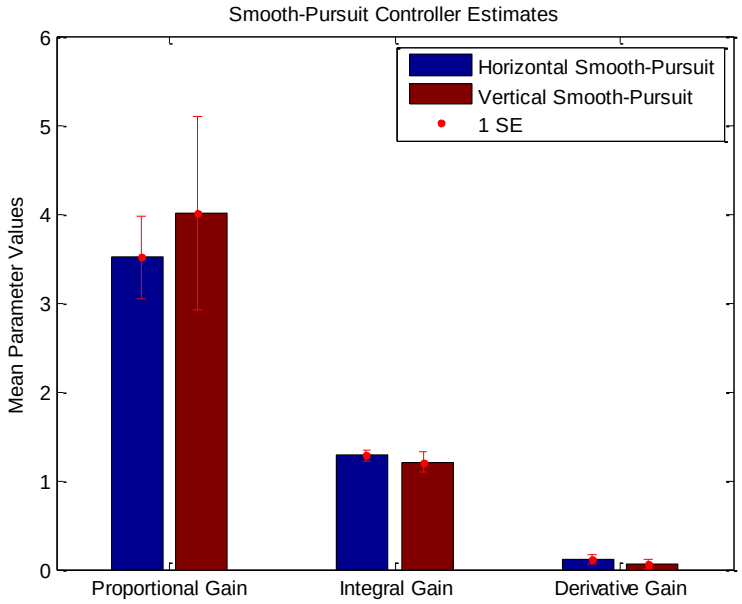

Figure 18: Average parameter estimates across subjects for smooth-pursuit controller gains. The gains estimated from the horizontal (blue) and vertical (red) smooth-pursuit tasks were consistent within and across subjects. No preferential axis of movement was observed in the smooth-pursuit sub-model.

Fitting to the time-series of the smooth-pursuit tasks yielded average R^2 values of 0.983 and 0.966 across all subjects for horizontal and vertical smooth-pursuit, respectively. The higher correlation values for the smooth-pursuit tasks are consistent with smaller overshoots, compared to the saccade tasks.

Across subjects, there was a generally a preference for higher horizontal gains. However, paired t-tests showed no statistical difference between any of the gains (proportional gain: t(12.12)=-0.35, p=0.73; integral gain: t(15.90)=0.30, p=0.77; derivative gain: t(15.92)=0.67, p=0.511) across the axial components.

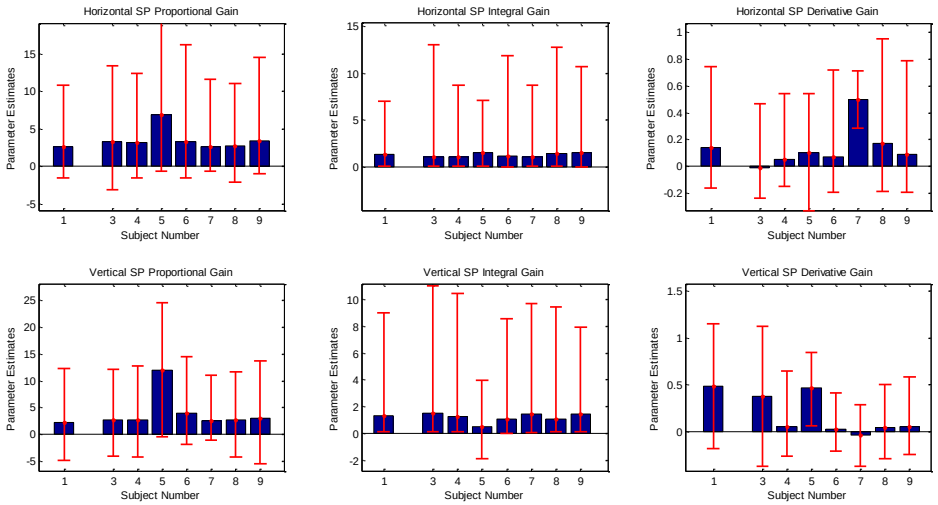

Figure 19: PID Gains for the best-fit smooth-pursuit (SP) controllers across subjects. Solid red lines indicate the 95% intervals of the parameter fits. Each subject's parameter was fitted with 1000 samples and all showing R^2 values > 0.95 between the subject data and best-fit model's response.

The specificity of model predictions using the best-fit controller parameters from each subject suggest the model can detect individual differences in subjects' eye

movement responses, when compared to the average best-fit parameters across all subjects. Figure 20 shows an example time-series from two subjects. EM_S05's

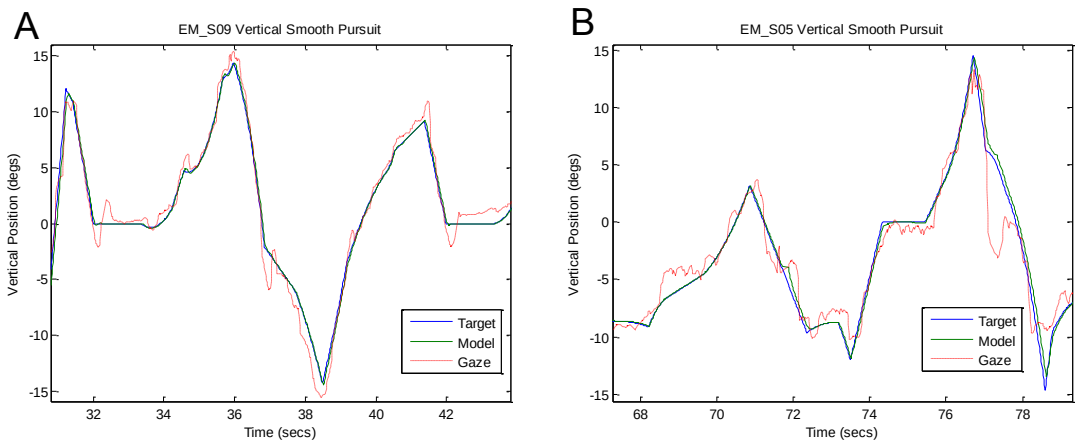

Figure 20: Sample time-series for vertical smooth-pursuit movements for subjects (A) EM_S09 and (B) EM_S05. The solid blue and green lines denote the target position and best-fit model response, respectively. The measured gaze positions over time are shown in red. The smooth-pursuit movements from EM_S05 shows more overshoot about the target position, and the steady-state positional error minimization for EM_S05's best-fit model response is sub-par to the typical best-fit model represented as the best-fit model for EM_S09.

gaze during vertical smooth-pursuit exhibited systematic overshoot, EM_S09's gaze during vertical smooth-pursuit showed little if any overshoot. The proportional gain for EM_S05 was approximately three times as large for vertical eye movements compared to the average gain across all subjects, while the integral gain was about half as large for vertical eye movements compared to the average value across subjects. The relative increase in proportional gain and decrease in integral gain suggests the subject utilized a control strategy where speed was prioritized over accuracy. This is supported by Figure 20 where EM_S05' best-fit model response showed more overshoot than the typical best-fit response represented by EM_S09.

4.2.3 2-D Interaction Parameters

To examine the interaction between the horizontal and vertical eye movements, the model was fit to subjects' responses to the 2-D (oblique) saccade and smooth-pursuit tasks. Table 3 and Table 4 show the best-fit parameter values (by subjects) characterizing the system interactions between horizontal and vertical position and velocity during saccade and smooth-pursuit eye movements. Positive values indicate horizontal eye movements accentuate either the magnitude of vertical eye position or the magnitude of vertical eye velocity (and *vice versa*). Negative values indicate that horizontal eye movements attenuate the same aspects of vertical eye movements (and *vice versa*). In addition to the parametric statistical metrics, the relative mean absolute error (RMAE) was used to characterize the model output's sensitivity to each parameter (Equation 4.3, where MAE_R is the mean absolute error with the parameter removed from the model and MAE_F is the mean absolute error with the full model). From

$$RMAE = \frac{(MAE\_R - MAE\_F)}{MAE\_F} * 100 \qquad (4.3)$$

Table 3, the interaction gains indicate that subjects tended to increase their eye velocity as a function of cross-axial eye position, such that changes in horizontal position pushed the eye vertically outward (upward and downward) for the saccade task. Conversely, the smooth-pursuit task showed that more medial eye positions increased cross-axial velocities, and that vertical velocity increased horizontal velocity.

	2-D Saccade Task							
Subject Number	$A^{\text{v-pos}}_{\text{h-pos}}$	$A^{\text{v-vel}}_{\text{h-pos}}$	$A^{\text{v-pos}}_{\text{h-vel}}$	$A^{\text{v-vel}}_{\text{h-vel}}$	$A^{\text{h-pos}}_{\text{v-pos}}$	$A^{\text{h-vel}}_{\text{v-pos}}$	$A^{\text{h-pos}}_{\text{v-vel}}$	$A^{\text{h-vel}}_{\text{v-vel}}$
1	0.004	0.001	0.552	0.032	0.011	0.003	0.093	-0.020
3	-0.001	-0.002	0.117	-0.007	0.002	-0.001	0.110	-0.001
4	0.003	0.000	0.333	0.069	0.002	0.000	0.217	-0.019
5	0.001	0.001	0.157	0.014	0.006	-0.001	0.088	0.009
6	-0.006	-0.003	0.177	0.041	-0.002	-0.003	0.190	0.001
7	0.002	-0.001	0.191	0.021	0.001	-0.001	0.084	-0.001
8	0.004	0.001	0.134	-0.011	0.007	0.001	0.157	0.003
9	-0.002	-0.003	0.185	-0.010	0.004	-0.003	0.071	-0.025
Avg	**0.001**	**-0.001**	**0.231**	**0.019**	**0.004**	**0.000**	**0.126**	**-0.007**
Std	*1.09E-03*	*5.85E-04*	*4.84E-02*	*9.39E-03*	*1.34E-03*	*6.89E-04*	*1.83E-02*	*4.31E-03*
t-value	0.5475	1.1517	4.4936	1.8713	2.6048	0.6267	6.5082	1.4671
p-value	0.6010	0.2872	0.0028	0.1035	0.0352	0.5507	0.0003	0.1858
df	7	7	7	7	7	7	7	7
RMAE Avg	0.090	-0.609	-0.038	0.163	0.436	-0.626	-0.043	-0.049
RMAE Ste	0.063	0.163	0.057	0.084	0.275	0.440	0.070	0.036
	2-D Smooth-Pursuit Task							
Subject Number	$A^{\text{v-pos}}_{\text{h-pos}}$	$A^{\text{v-vel}}_{\text{h-pos}}$	$A^{\text{v-pos}}_{\text{h-vel}}$	$A^{\text{v-vel}}_{\text{h-vel}}$	$A^{\text{h-pos}}_{\text{v-pos}}$	$A^{\text{h-vel}}_{\text{v-pos}}$	$A^{\text{h-pos}}_{\text{v-vel}}$	$A^{\text{h-vel}}_{\text{v-vel}}$
1	0.000	-0.003	0.025	0.004	0.000	-0.002	0.003	0.000
3	0.001	-0.003	0.003	0.001	0.000	-0.002	0.002	0.001
4	-0.002	-0.004	0.172	0.043	0.002	-0.004	0.128	0.035
5	-0.001	-0.003	0.003	0.002	0.001	-0.004	0.000	-0.001
6	0.000	-0.003	0.034	0.025	0.000	-0.004	0.078	0.019
7	-0.001	-0.002	0.011	0.003	-0.001	-0.002	0.001	0.001
8	0.000	-0.004	0.032	0.010	0.000	-0.003	0.006	0.003
9	-0.001	-0.003	0.049	0.011	0.001	-0.003	0.021	0.011
Avg	**-0.001**	**-0.003**	**0.041**	**0.012**	**0.000**	**-0.003**	**0.030**	**0.009**
Ste	*2.65E-04*	*1.83E-04*	*1.84E-02*	*4.81E-03*	*2.94E-04*	*2.70E-04*	*1.58E-02*	*4.19E-03*
t-value	1.7895	15.8956	2.1046	2.4044	1.1816	10.2774	1.7793	1.9796
p-value	0.1167	9.46E-07	0.0734	0.0472	0.2760	1.79E-05	0.1184	0.0882
df	7	7	7	7	7	7	7	7
RMAE Avg	0.466	1.326	0.517	0.055	0.057	-0.090	0.011	0.018
RMAE Ste	0.397	0.523	0.459	0.037	0.057	0.131	0.026	0.021

Table 3: 2-D plant interaction parameters for 2-D saccade and smooth-pursuit tasks. For each parameter, the average (Avg), standard error (Ste), t-value, p-value and degrees of freedom (df) were computed across subjects. The relative mean absolute error (RMAE) characterizes the change in model error (actual response – model response) when the parameter in that column is removed from the model. Parameters where values were significant ($p<0.05$) are shown in red, regardless of the RMAE.

	2-D Saccade Task			
Subject Number	$B^{v\text{-}e}_{h\text{-}pos}$	$B^{v\text{-}e}_{h\text{-}vel}$	$B^{h\text{-}e}_{v\text{-}pos}$	$B^{h\text{-}e}_{v\text{-}vel}$
1	0.004	0.133	0.002	-0.065
3	0.000	-0.240	-0.001	-0.201
4	0.015	-0.318	0.006	-0.048
5	0.004	0.172	0.003	0.143
6	0.007	-0.189	0.006	-0.103
7	0.003	-0.027	0.000	-0.177
8	0.002	-0.071	0.004	0.133
9	0.004	-0.217	0.003	-0.191
Avg	**0.005**	**-0.095**	**0.003**	**-0.064**
Ste	*1.48E-03*	*5.95E-02*	*8.82E-04*	*4.56E-02*
t-value	3.1496109	1.4996651	3.1241845	1.3154151
p-value	0.0161608	0.1773831	0.0167454	0.2298164
df	7	7	7	7
RMAE Avg	0.762	-0.237	0.499	0.078
RMAE Ste	0.369	0.100	0.218	0.132
	2-D Smooth-Pursuit Task			
Subject Number	$B^{v\text{-}e}_{h\text{-}pos}$	$B^{v\text{-}e}_{h\text{-}vel}$	$B^{h\text{-}e}_{v\text{-}pos}$	$B^{h\text{-}e}_{v\text{-}vel}$
1	0.000	-0.038	0.000	-0.043
3	0.000	0.008	0.001	-0.017
4	0.002	-0.073	0.006	0.105
5	0.000	-0.026	0.001	-0.008
6	0.001	0.002	0.002	0.028
7	0.001	-0.049	0.001	-0.017
8	0.000	-0.040	0.001	-0.033
9	0.000	-0.059	0.001	0.014
Avg	**0.001**	**-0.034**	**0.002**	**0.004**
Std	*2.58E-04*	*9.36E-03*	*5.75E-04*	*1.58E-02*
t-value	2.3094428	3.4542107	2.4739448	0.21118
p-value	0.0542313	0.0106305	0.0425862	0.8387632
df	7	7	7	7
RMAE Avg	0.017	0.004	0.054	-0.009
RMAE Ste	0.011	0.008	0.025	0.013

Table 4: 2-D error-driven interaction parameter summary for 2-D saccade and smooth-pursuit tasks. Row labels are the same as in Table 3.

The interaction between horizontal and vertical eye movements characterized by the error-driven ocular dynamics gains (Table 4), indicates a tendency for the position error to push the cross-axial position outward for the saccade task. In the smooth-pursuit task vertical error slowed down horizontal velocity, while the horizontal error pushed the eye vertically outward.

For the saccade task, the influence of position on the cross-axial velocity was shown to be positive and significant ($A^{v\text{-}pos}_{h\text{-}vel}$ and $A^{h\text{-}pos}_{v\text{-}vel}$; $p<0.005$) for both horizontal and vertical components of the 2D eye movement. As the eye moved outward, speed along the perpendicular direction increased. However, functionally the impact of the interaction on the model response was relatively low, with relative mean absolute errors (RMAE) of -0.038 for the horizontal direction and -0.043 for the vertical direction.

In contrast, the influence of horizontal position (and position error) on vertical position, and the influence of vertical error on horizontal position were less significant ($A^{h\text{-}pos}_{v\text{-}pos}$, $B^{h\text{-}e}_{v\text{-}pos}$ and $B^{v\text{-}e}_{h\text{-}pos}$; $0.01<p<0.05$), but showed greater impact on the model response ($RMAE\geq0.5$). One practical impact on model performance was to increase vertical eccentricity (distance from center) as a function of horizontal eye position. The other impacts on model performance were to increase horizontal eccentricity as a function of vertical error and to increase vertical eccentricity as a function of horizontal error resulting in more outward eye positions for inaccurate goal-directed movements.

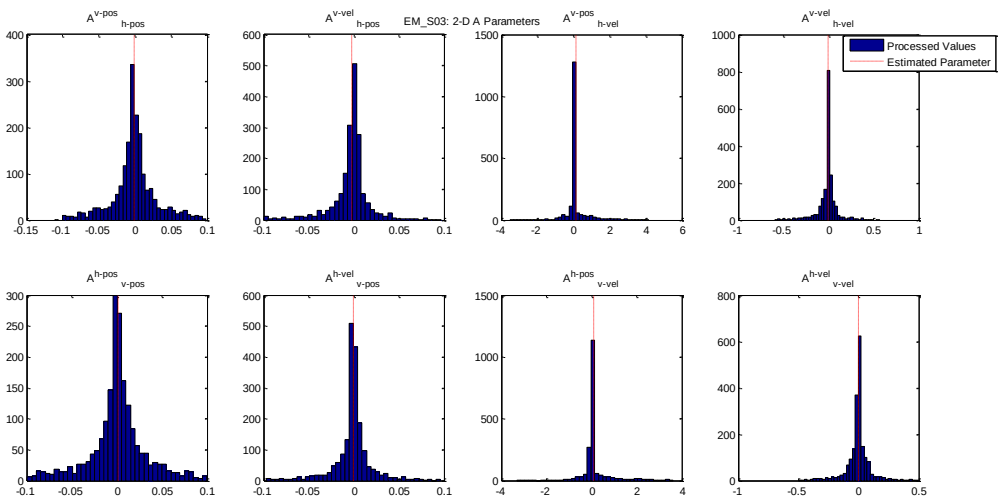

Figure 21: Distributions of best-fit system interaction parameters for EM_S03 (n>1000) using the 2-D Saccade task. Blue bars indicate the number of parameter estimated in each bin. Dashed red lines indicate the best-fit mean estimate for each parameter obtained from the box-cox transformation.

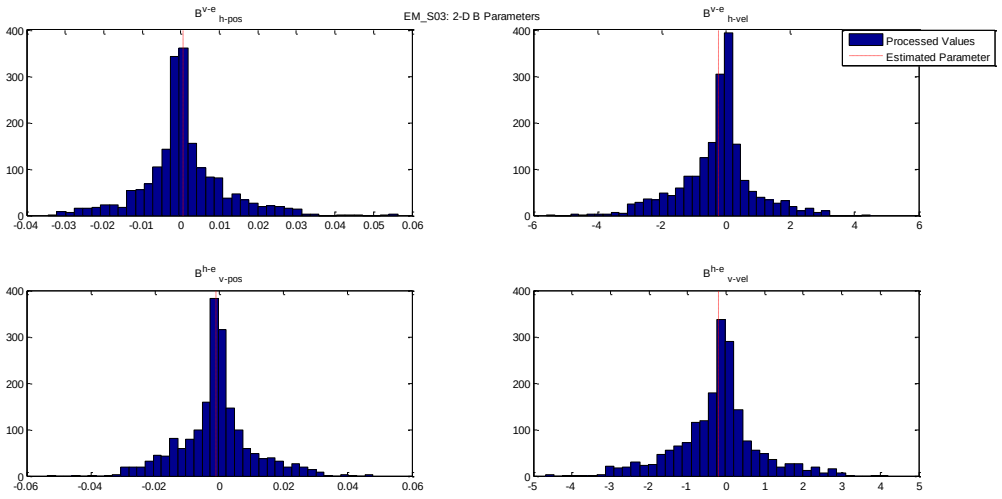

Figure 22: Distributions of best-fit error-driven system interaction parameters for EM_S03 (n>1000) using the 2-D Saccade Task. Labeling is the same as in Figure 21.

The smooth-pursuit task yielded different interactions. The influence of velocity on cross-axial position for the horizontal and vertical directions were both highly significant ($A^{v\text{-}vel}_{h\text{-}pos}$ and $A^{h\text{-}vel}_{v\text{-}pos}$; $p<0.0001$) and had the greatest effect on simulated eye

position (RMAE≥0.09). The negative sign associated with the coefficient meant that increasing horizontal or vertical velocity pushed the eye medially (inward). Other significant interactions included a proportional increase in horizontal velocity with vertical velocity ($A^{v\text{-}vel}_{h\text{-}vel}$; p=0.047), a decrease in vertical error slowing with horizontal velocity ($B^{v\text{-}e}_{h\text{-}vel}$; p=0.011) and a vertical outward shift in eye position with horizontal position error ($B^{h\text{-}e}_{v\text{-}pos}$; p=0.043). Some significant interactions, such as $A^{v\text{-}vel}_{h\text{-}vel}$, $B^{v\text{-}e}_{h\text{-}vel}$ and $B^{v\text{-}e}_{h\text{-}vel}$ showed relatively less effect on the model (RMAE≤0.055) compared to other significant interactions, such as $A^{v\text{-}vel}_{h\text{-}pos}$ and $A^{h\text{-}vel}_{v\text{-}pos}$, suggesting that 2-D interactions of eye velocity on eye position are more discernible than interactions of eye position on eye velocity during smooth-pursuit eye movements.

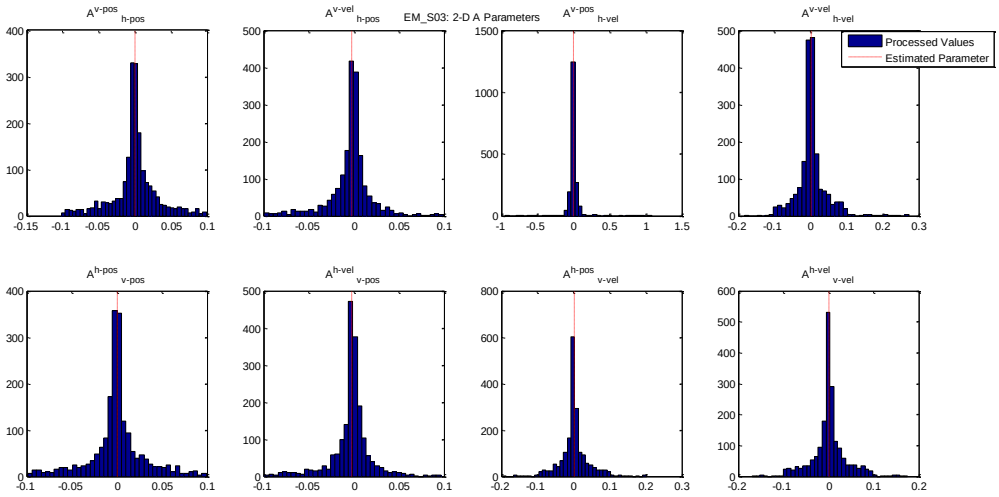

Figure 23: Distributions of best-fit system interaction parameters for EM_S03 (n>1000) using the 2-D Smooth-Pursuit Task. Labeling is the same as in Figure 21.

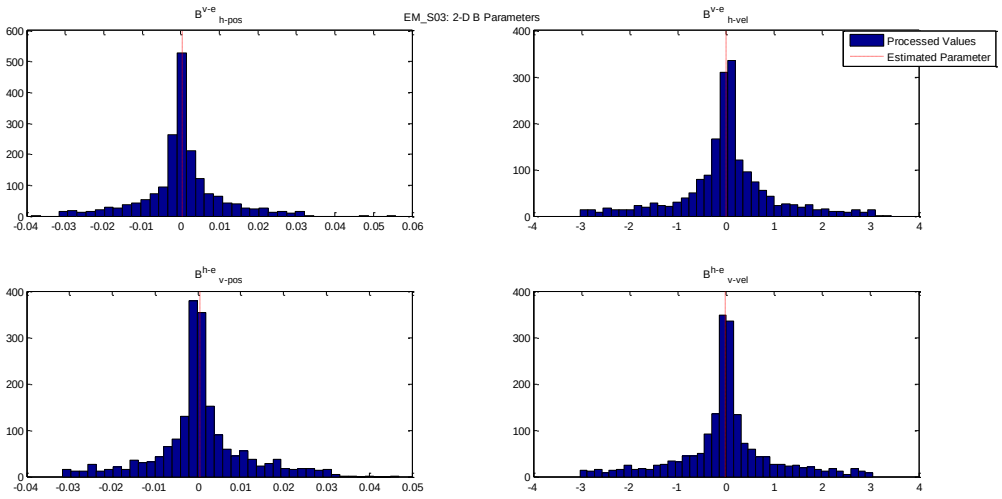

Figure 24: Distributions of best-fit error-driven system interaction parameters for EM_S03 (n>1000) using the 2-D Smooth-Pursuit Task. Labeling is the same as in Figure 21.

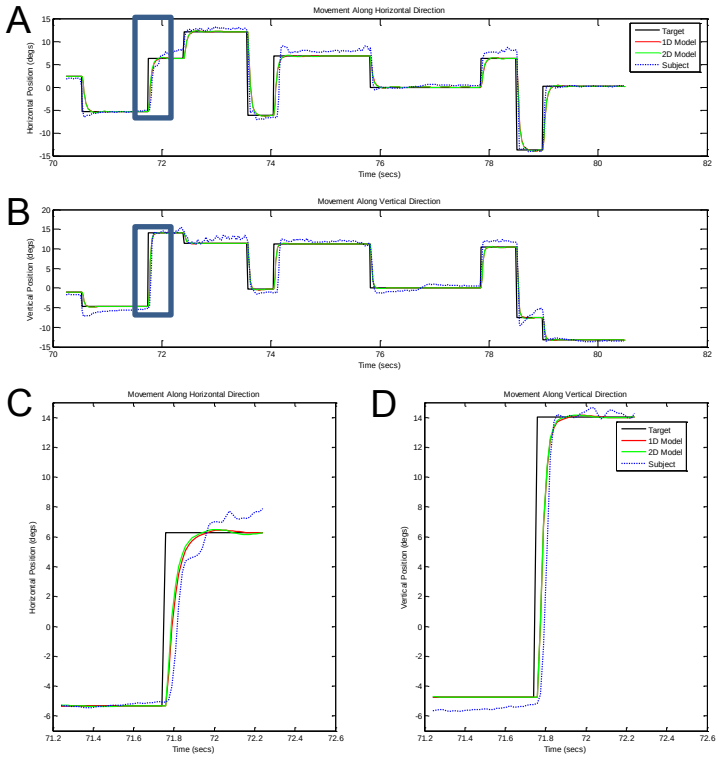

Figure 25: Effects of 2-D system interactions on saccade response for EM_S09. The model response shown here is the best-fit model for EM_S09. Each subplot shows the target (solid black line), EM_S09's visual response (dashed blue line), the best-fit model response for a 1-D model response (all interaction parameters are zeroed; solid red line) and 2-D model (significant interaction parameters are enabled; solid green line). Subplots C and D show exploded views of responses in A and B indicated by the blue boxes.

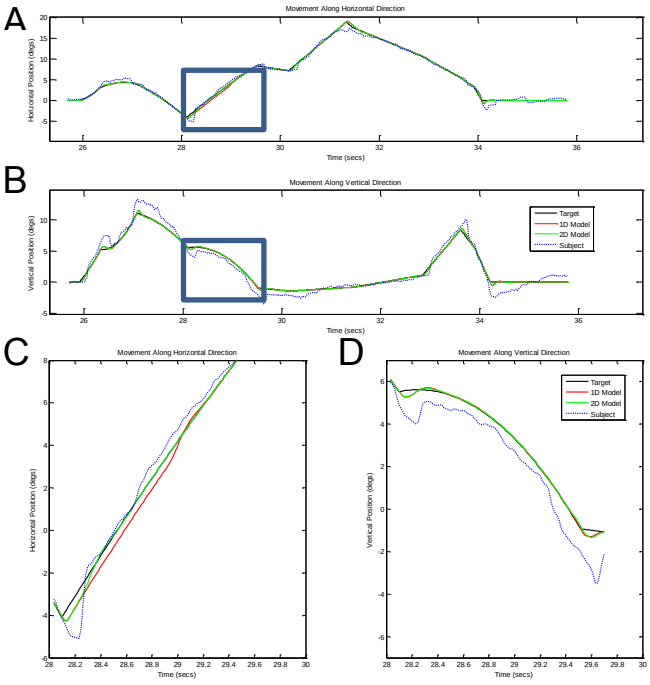

Figure 26: Effects of 2-D system interactions on smooth-pursuit response from EM_S09. Labeling is the same as in Figure 25.

Figure 27 shows the correlation (R^2) between subjects' individual response and the corresponding best-fit model together with the root mean square error (RMSE),

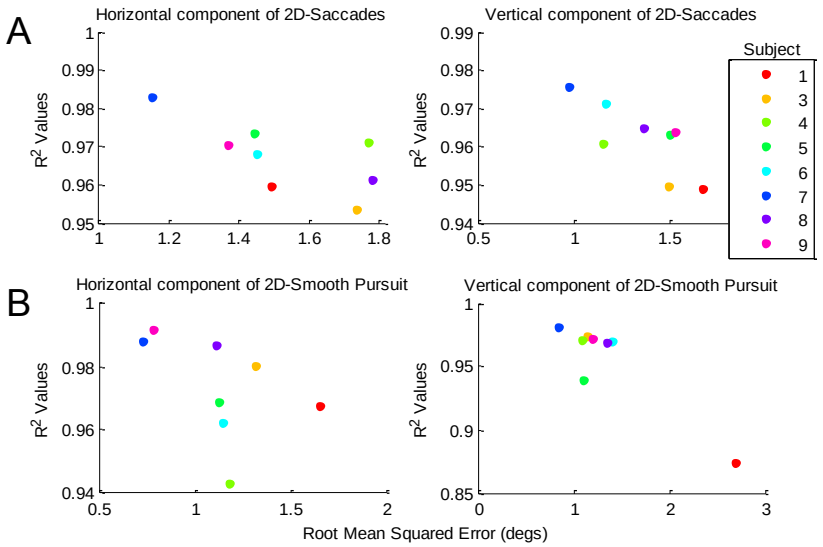

Figure 27: Goodness of fits for 2-D interaction parameters under training data for (A) saccade data and (B) smooth-pursuit data. The correlation (R^2) and root mean squared error values were computed between the model response and subject gaze for each set of trials of a given task.

for all subjects, axial components and tasks. Typically, the R^2 and RMSE metrics show an inverse relationship with high R^2 and low RMSE values for good fits between two data sets. Deviations from this relationship reveal characteristics about the model-fitting process. Figure 27 shows that the horizontal saccade and smooth-pursuit eye movements had different R^2 values for similar RMSE values (more so than multiple RMSE values for similar R^2 values), indicating greater sensitivity to temporal errors than spatial errors (positional error between best-fit model and subject responses). The vertical component of the movements had different RMSE values for similar R^2 values, resulting from greater sensitivity to spatial errors.

It should be noted that temporal mismatches between the model and subject saccades dominated the high RMSE values (Figure 28), where position transitions during saccades can produce an error up to 20˚. Errors of this magnitude give more weight to points associated with saccades when computing the average error across a data set,

resulting in accentuated RMSE values. Errors resulting from saccadic position errors are influenced by errors in temporal matching between the subject and model output positions, with the lag size contributing a multiplicative effect on the error. Thus, the seemingly high RMSE values may be reduced in future studies for eye tracking systems with higher resolution and improved algorithms for temporally aligning the subject and model output positions.

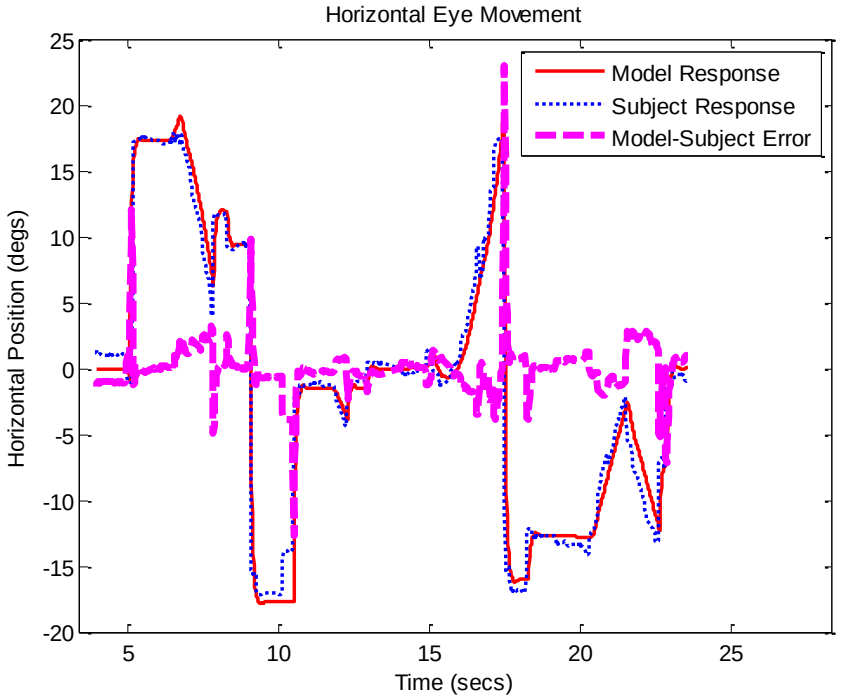

Figure 28: Sample subject (EM_S06) and model responses from the combined saccade and smooth-pursuit task. The red and blue lines indicate the best-fit model's position and subject gaze position, respectively, in response to both discrete and continuous targets. The magenta line represents the point-by-point positional error between these two signals. The error is consistently larger in magnitude for saccades than for smooth-pursuit eye movements.

Table 5 shows the average metrics across all subjects for 1-D and 2-D saccade and smooth pursuit. Paired t-tests between the metrics of 1-D saccade and 1-D smooth-pursuit, 2-D saccade and 2-D smooth-pursuit, 1-D saccade and 2-D saccade, and 1-D smooth-pursuit and 2-D smooth-pursuit tasks were computed to show the influence of

tasks on model fitting performance, with the latter two comparisons indicating how well the 2-D data are modeled by independent 1-D controllers. The difference in RMSE between the 1-D saccade and 1-D smooth-pursuit tasks was significant ($t(30)=2.56$, $p=0.016$) as expected, however, the other comparisons were not ($p>0.05$), indicative of the model's consistency in fitting to saccade and smooth-pursuit eye movements across the 2-D space and inconsistency across the 1-D space.

	Horizontal Component	Vertical Component
Saccade - RMSE (degs)	1.377 (±0.08)	1.338 (±0.10)
Saccade - R^2	0.972 (±0.01)	0.957 (±0.01)
Smooth-pursuit - RMSE (degs)	0.929 (±0.09)	1.262 (±0.11)
Smooth-pursuit - R^2	0.984 (±0.01)	0.967 (±0.01)
2-D Saccade – RMSE (degs)	1.524 (±0.078)	1.360 (±0.084)
2-D Saccade – R^2	0.967 (±0.003)	0.962 (±0.003)
2-D SP – RMSE (degs)	1.132 (±0.103)	1.351 (±0.201)
2-D SP – R^2	0.974 (±0.006)	0.956 (±0.013)

Table 5: Goodness of Fit Summary for the Controller Parameters. Metrics shown here are averages and standard errors computed across all subjects.

4.3 Model Performance Evaluation

The performance of the best-fit model for each subject was evaluated using the responses from the 2-D dual-movement tasks as experimental test data. Five trials from each subject's data set were selected and concatenated using the criteria and procedures outlined in section 3.5.1 to reduce variability in data length between the training and testing data. The models were evaluated under two conditions: delays removed and delays intact from the experimental data. Removing the delays from each trial using cross-correlation, while zeroing the subject-specific delay parameters, eliminated variability caused by delay estimations. Keeping the delays from the experimental data, while implementing the subject-specific delay estimations to the model, tests the variance

introduced by the delay estimations. For each condition, the dead zone for saccade onset was set to 0.5˚. The correlation and root mean squared error between the subjects' responses and the best-fit model were used to compare the best-fit model to the subject gaze.

4.3.1 Model Performance without Delay Estimations

Figure 29A shows the correlations and root mean squared errors for the horizontal and vertical components of the 2-D eye movements across subjects. Performance on the

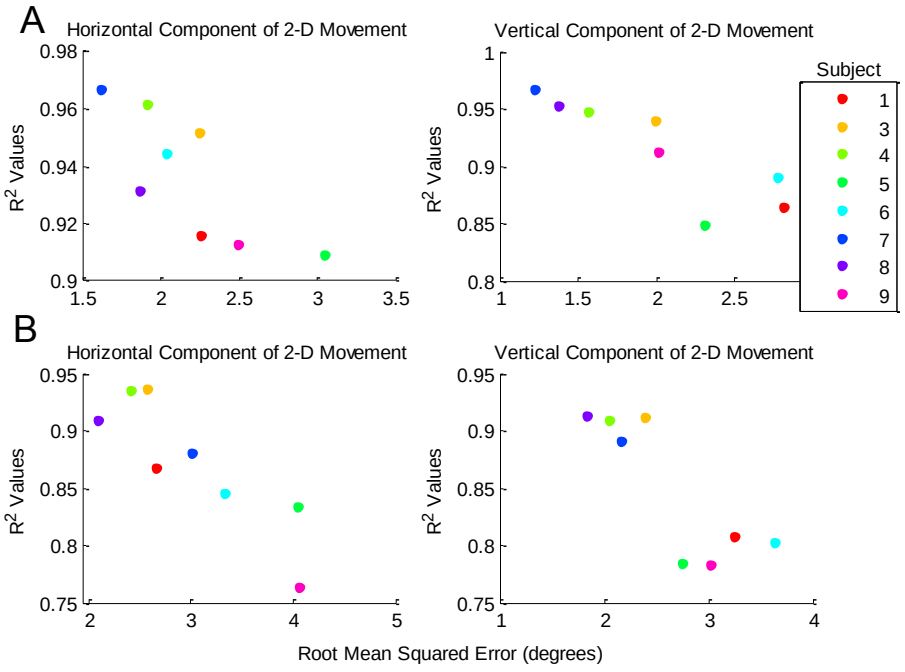

Figure 29: Model Validation using subject-specific best-fit models with test data. A) Delay-exclusive condition: the delays were removed from test data using cross-correlation and only the fitted parameters are tested here. B) Delay-inclusive condition: with subject gaze delays intact, the subject-specific estimated delays for the model are tested along with the fitted parameters. Including the delays into the validation analysis generally increased root mean squared error and decreased correlation.

test data showed lower correlations and higher root mean squared errors than the training data in Figure 27, suggesting that the data sets have an influence on the best-fit model estimation.

4.3.2 Model Performance with Delay Estimations

Figure 29B shows the correlations and root mean squared errors between the delay-inclusive conditions for each subject. The lower correlations and higher errors show that the model performed with less accuracy in this condition than in the delay-exclusive condition. The lower correlations imply that the delays interfered with the model's ability to predict the subject's response. Figure 30 shows sample time-series for

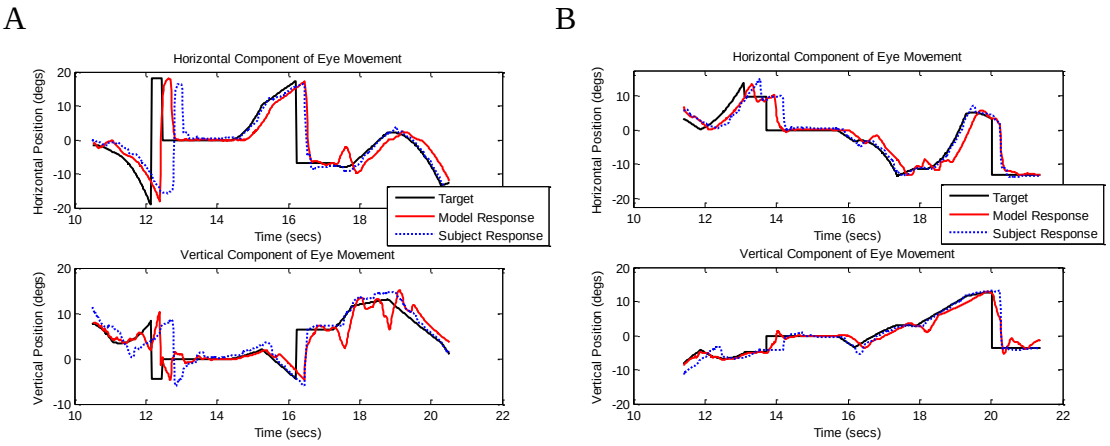

Figure 30: Sample time-series from 2-D dual-movement tasks for model validation with delays included. A) EM_S09's data and best-fit model response, which showed the lowest correlation across all subjects. B) EM_S04's data and best-fit model response, which showed the highest correlation across subjects. In both (A) and (B), inconsistent differences between the model and experimental delays are due to inconsistent delays from subject responses that affected the delay estimation for the trial.

subjects whose best-fit models, along with delay estimations, showed lowest and highest correlation values between subject and best-fit model responses. The contrast in model response accuracy between the two subjects shows a correlation range of 0.75-0.95.

Considering the range of positive correlation values is 0-1, corresponding to no relationship and a perfectly linear relationship, respectively, the correlations indicate that the models can account for the subject responses even for test data.

As expected, the model's goodness of fit decreased across all subjects when fitted to testing, or untrained, data consisting of 2-D saccade and smooth-pursuit sub-targets (Table 6). T-tests revealed significant differences between the performance metrics

	Horizontal Component	Vertical Component
Training Data – RMSE (degs)	1.328 (±0.196)	1.356 (±0.005)
[1]Testing Data – RMSE (degs)	2.183 (±0.149)	2.007 (±0.200)
[2]Testing Data – RMSE (degs)	2.987 (±0.252)	2.627 (±0.210)
Training Data – R^2	0.971 (±0.004)	0.959 (±0.003)
[1]Testing Data – R^2	0.937 (±0.007)	0.916 (±0.015)
[2]Testing Data – R^2	0.874 (±0.020)	0.852 (±0.020)

Table 6: Goodness of Fits Summary. Training data yielded the lowest root mean squared error (RMSE) and highest correlation between model output and actual subject data. Both goodness of fit metrics became progressively worse for [1]Testing Data, or delay-exclusive data where cross-correlation reduced delays, and [2]Testing Data, or delay-inclusive data where delay estimates were evaluated as well.

of the three different data types ($p<0.05$), except for the horizontal RMSE between the delay-exclusive ([1]Testing Data) and delay-inclusive ([2]Testing Data) delay conditions ($t(14)=2.1$, $p=0.05$). The model performance under the delay-inclusive condition was less accurate than the delay-exclusive condition, likely resulting from the additional variance to the best-fit model due to the delay estimations, which suggests that increasing the number of parameters to be fit decreases the performance accuracy of the model to testing data. It is unlikely that the difference between these conditions reflects inconsistently computed delays resulting from experimental attention and fatigue, since those delays are also used in the delay-exclusive condition (to align subject data to target).

5. DISCUSSION

For the 1-D analysis of saccade and smooth-pursuit eye movements, although parameters characterizing the horizontal and vertical eye movements were not statistically different, trends in the parameter estimates characterized higher velocities in vertical versus horizontal saccades and more overshoot in the vertical versus horizontal smooth-pursuit eye movements. The parameter estimates suggest that the model can characterize eye movement characteristics such as speed and overshoot, but a larger sample size of subjects or a higher resolution eye tracking system may be required to classify statistically significant effects across subjects. The analysis of 2-D eye movements suggest a variety of position-based and velocity-based interactions between horizontal and vertical eye movements based on parameter estimates across subjects. However, the effect of these interactions on the functional response were generally small, and both quantitative (best-fit parameter estimates) and qualitative (functional responses) results should be considered to investigate the independent control hypothesis clearly.

5.1 Delay and Dead zone Analyses

5.1.1 Delay Estimates

The experimental estimates of saccade and smooth-pursuit eye movement latencies (242± 24 ms and 107± 33 ms respectively) was generally high but fell within the margin of error reported across previous studies. An earlier study on saccadic eye movements reported latency ranges of 200-250 ms (Yang, Bucci, & Kapoula, 2002), while another reported a mean of 211 (± 8) ms for healthy adults (Rashbass, 1961).

Latency estimates for both movement types may have been influenced by an unresolved delay between the target and subject gaze markers. For each trial, markers,

from the stimuli-generating computer, corresponding to the onset of each trial's first target were sent to the Arrington ViewPoint software to temporally align stimuli and gaze positions. The temporal mismatch may arise from time-consuming computational tasks performed after the marker is sent but before the actual onset of the trial's first target. However, whether these delays had a large effect on computations of eye movement latencies is questionable because only the saccade latency is slightly inconsistent with reported values from literature. An issue with the marker delays would have affected both saccade and smooth-pursuit latencies equally, and the consistency of the smooth-pursuit latencies with values from literature suggests the size of the marker delays is negligible.

The error in the saccade latency estimates could also result from a non-optimal saccade detection algorithm. The implemented algorithm required eye position displacements to exceed 50% of the corresponding sub-target step displacement before a saccade is detected and recorded. Since the duration of saccades ranged 37-45 ms for 8-10˚ displacements (Collins, Semroud, Orriols, & Dore-Mazars, 2008), in many cases saccades were defined by two or three data points due to the 60 Hz temporal resolution of the eye tracker. The limited temporal resolution resulted in saccade latencies with a minimum error of 16 ms. Coupled with the method used to detect saccade onset, this suggests that the saccade latencies may have been overestimated. This did not impact the subsequent model fits since the delays were removed as a result of temporal alignment of subject gaze to target position.

5.1.2 Dead Zone Estimates

Our estimates for the horizontal and vertical dead zones of 0.027 (±0.034)˚ and 0.0133 (±0.009)˚ showed 94.6 (±3.14) % and 97.3 (5.02) % differences from the reported 0.5˚ (L. R. S. Young, L, 1963). Using our estimated dead zones of 0.027˚ and 0.0133˚, the model output would be dominantly controlled by the saccade branch for all sub-target displacements.

The errors in estimated dead zones are most likely due to the eye tracker noise and saccade detection techniques. The resolution of the Arrington eye tracker is comparable to the saccade threshold reported in literature, making accurate estimates difficult. The saccade detection algorithm registered eye movements as saccades if the eye position displacements exceeded 50% of corresponding target displacements. Although this method was an attempt to disqualify noise measurements from detected saccades, the 50% threshold for saccade detection was arbitrary and was too sensitive for detecting saccades. Lower threshold values risk more false saccade detections, while the dead zone estimation did not change for higher threshold values. A lower bound of 0˚ for sub-target displacements also contributed to the low dead zone values (see Section 4.1.2), and implementing a lower bound equal to the estimated eye tracker noise level may limit dead zone detection to higher (and more reasonable) values.

5.2 Parametric Analysis

5.2.1 Initial-Model

The initial-model was able to replicate two common characteristics of human saccade and smooth-pursuit eye movement: the main sequences, shown in Figure 1 and

Figure 7. The model showed a saturating linear relationship between peak velocity and saccade magnitude for saccades ranging 0˚-35˚, and exhibited a linear relationship between peak acceleration and smooth-pursuit velocity. Earlier studies showed nonlinear relationships for saccade distances greater than 20 degrees, assuming that glissades are classified as saccades in this study. Removing the velocity saturation in this model (based on pilot data) showed a linear relationship above those bounds, but it did not affect our subsequent parametric analysis, as the 60 Hz temporal resolution of the eye tracker system may have underestimated the actual peak velocities due to single saccades being represented by as few as 2 points. However, the model was able to replicate the peak velocities and accelerations from the pilot study, seen in Figure 7 C-F. The resemblance to pilot data indicates that the parameters from the normative model produced stable saccade and smooth-pursuit responses to visual targets.

5.2.2 Saccade Control

To our knowledge, only one study has modeled saccades with PD control (Chen-Harris et al., 2008). However, the control parameters varied adaptively over the course of a trial and values were not reported. Thus, the accuracy of the estimated control gains in our model was evaluated through comparison to subjects individual eye movements using the correlation and root mean squared error between the fitted model output and subject gaze (Table 5). The high linear relationship between the model and actual data suggests the PD control was sufficient to capture the temporal characteristics (temporal lag between model and subject gaze) of the subjects' gaze. The RMSE values of 2.031 (±0.084) and 2.024 (±0.281) degrees between the model response and subject gaze from testing data are more than three factors outside of the 0.5˚ dead zone, suggesting that the

model did not spatially match the subjects' gaze (offset errors between model and subject gaze) as well as it did for the temporal characteristics as suggested by high root mean squared error versus high correlation.

Previous studies have reported saccade characteristics for horizontal and vertical eye movements that compare unfavorably to our 1-D saccade analysis (Becker & Jurgens, 1990; Collewijn, Erkelens, & Steinman, 1988a, 1988b). Although not statistically significant ($t(14)=0.85$, $p=0.41$ and $t(14)=0.07$, $p=0.95$), the proportional gain was typically larger for vertical than for horizontal eye movement, suggesting more likelihood to overshoot the target. Typically smaller derivative gains for vertical versus horizontal saccades suggest. Collewijn's study showed lower maximum speeds for vertical saccades up to 40 degrees by approximately 15% than for horizontal saccades of similar amplitudes (Collewijn et al., 1988a, 1988b). Becker and Jurgens also showed slower vertical saccades than horizontal saccades (Becker & Jurgens, 1990). The subject gaze movements here, encompassing a 36 degree visual range, tended to show faster vertical saccades than horizontal saccades although the effect was not significant. For example, EM_S09 showed approximately 20% higher velocities for vertical versus horizontal saccades. Figure 31 shows a sample subject's gaze data, whose overshoot is more observable for vertical versus horizontal eye movements although similar observations were made for the other subjects. The differences in horizontal and vertical saccade speeds may be influenced by the pitch of the subjects' head relative to the screen, where a lower pitch causes the subject to look up to fixate on the screen center resulting in more downward versus upward saccades. An earlier study showed that downward saccades showed higher velocities than upward saccades (Collewijn et al., 1988b), and if

some subjects positioned their head at a lower pitch, the higher probability of downward saccades explains higher velocities for vertical versus horizontal saccades.

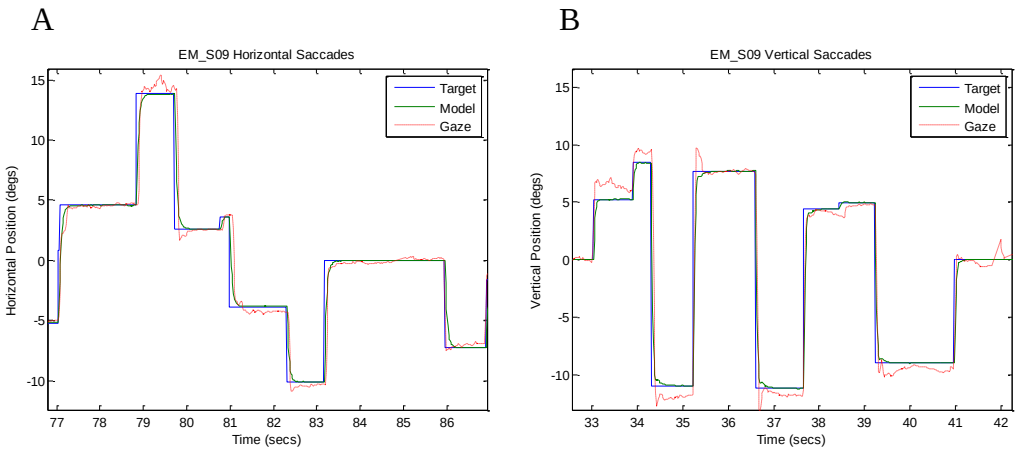

Figure 31: Sample time-series (EM_S09) for 1-D (A) horizontal and (B) vertical saccades. Target position is shown in blue. The model output and subject gaze positions are shown in green and red respectively. Positional offsets of about 2˚ are more prevalent for vertical saccades than for horizontal saccades.

The differences in control gains between horizontal and vertical saccade control may be influenced by the experimental setup. The eyelids can limit the measurable range of vertical eye movements. Yee and colleagues found that that measurements of vertical eye position saturated at 10˚ above and 20˚ below screen center for most subjects using an infrared eye tracker (Yee et al., 1985). When eyelids interfere with the Arrington system, the eye tracker software attempts to find another round object in the camera view, which can result in misidentification of eye position or a registered eye blink. This issue may have contributed to the larger positional error in the vertical eye movement. Also, horizontal movement was limited to a range of motion of 37˚ while vertical movement was limited to 28˚, based on the asymmetry of the viewing monitor. Larger movements may have emphasized derivative over proportional control in order to move the eyeball

across longer distances over a short time and reduce error, which may explain why the horizontal saccade control showed larger derivative and smaller proportional gains compared to the vertical saccade control.

While additional subjects may be required to obtain sufficient statistical power across the population, the current results show the saccade control parameters' sensitivity to positional overshoot for saccades. This suggests that the saccade controller is sensitive to similar overshoot characteristics in saccade data seen with ocular dysmetria, a common visual condition in persons with MS.

Other studies have characterized saccades using different types of control, including bang-bang-step control (Bahill et al., 1975b), where horizontal position is determined by all-or-nothing signals in the left and right directions, or quasi-bang-bang-step (pulse-step) where the maximum was amplitude-sensitive (Winters, Nam, & Stark, 1984). Pulse-step control, where saccade onset is mediated by a high constant amplitude "pulse" signal and a lower amplitude "step" signal, has also been used to initiate a saccade and maintain steady-state position (Lesmana, 2011). Both of these are more physiologically correct for actuating the horizontally-active medial and lateral recti muscles and replicating the high velocities in saccades, but the PD controller is a more general model that is less computationally difficult to implement. The PD controller is also more closely related to the PID controller in smooth-pursuit control than the other controllers, allowing relationships between saccade and smooth-pursuit control to be more clearly understood.

5.2.3 Smooth-Pursuit Control

Unlike saccade control, smooth-pursuit control emphasizes speed and accuracy during closed-loop control and is often approximated as a PID controller in oculomotor control models (Balkenius & Johansson, 2005; Brown, 1989), where the addition of the integral gain is crucial for the minimization of steady-state error during closed-loop tracking. However, comparison of actual gain values is difficult due to a lack of reported values from literature.

Vertical smooth-pursuit eye movements have been observed to be less accurate than horizontal movements (Baloh, Yee, Honrubia, & Jacobson, 1988; Rottach et al., 1996). In the current study, PID gains were not significantly different for horizontal and vertical eye movements (P: $t(9)=0.40$, $p=0.70$; I: $t(11)=0.55$, $p=0.59$; D: $t(14)=0.68$, $p=0.51$). Despite insignificance, the integral and derivative gains, averaged across subjects (Figure 18), were generally higher for the horizontal versus vertical control, with the opposite relationship seen for the proportional gain. Previous studies have reported smaller target-eye phase lag during smooth-pursuit in the horizontal direction and higher accelerations during smooth-pursuit in the vertical direction (Baloh et al., 1988; Rottach et al., 1996). Based on these results, the proportional and integral gains were expected to be higher for the horizontal versus vertical control to emulate accurate horizontal tracking, and the derivative gain larger for vertical control to account for higher eye accelerations. This reveals the ambiguity of interpreting movement strategy based on PID gains as the effects of the gains on the movement dynamics can overlap, especially the proportional gain's influence on both movement speed and accuracy. Regardless of the interpretation of the individual control gains, a larger sample size of subjects would

be needed to determine parametrically if horizontal and vertical smooth-pursuit are statistically different.

5.2.4 2-D Interaction Control

Table 3 indicates an interaction between horizontal and vertical control, with horizontal position influenced by vertical position. However, Figure 32 shows the consistency of this interaction, where a perfect interaction of this type is represented by a V-shape of vertical positional error versus horizontal eccentricity (A) or *vice versa* (B). The figure indicates large variability in interaction of horizontal position on vertical position, where the scatter plot's deviation from a V-shape indicates inconsistency with the 0.007 best-fit value for EM_S08's parameter $A^{h\text{-}pos}_{v\text{-}pos}$ that simulates increasing overshoot in the vertical direction as the eye moves horizontally outward. To the best of our knowledge, this interaction has not been reported previously in literature. It is possible the best-fit 2-D models are affected by residual fitting errors from the 1-D model, especially with more pronounced vertical overshoots versus horizontal overshoots in the 1-D tasks as mentioned in section 5.2.2. Perhaps an unresolved eye tracker error that is sensitive to the vertical directions seen during the 1-D data could manifest in the 2-D data, resulting in larger overshoots in the vertical versus horizontal eye movements for both 1-D and 2-D data.

With regards to model evaluation, the model was oblivious to the eye tracker issues and whether eye movement characteristics were real or induced by experimental errors, and the resulting best-fit models can be used to measure the model's sensitivity to 2-D interactions. The interaction of horizontal position on vertical position was statistically significant (Table 3: $t(7)=2.60$, $p=0.035$), yet the quantitative impact of the

interaction was unclear (Figure 32: a V-shape corresponding to a perfect interaction between horizontal and vertical positions is not clearly shown), suggesting the system identification procedure was sensitive to small effects that may not be readily detected based simply on the subject's responses. Similarly, the interaction effects induced by the controllers on the horizontal and vertical positions ($B^{v\text{-}e}_{h\text{-}pos}$ and $B^{h\text{-}e}_{v\text{-}pos}$) were statistically significant (Table 4), however their impact on subject's actual eye movements appear to be minimal, seen by rotating Figure 32 by 90 degrees to show the interaction of positional error on position.

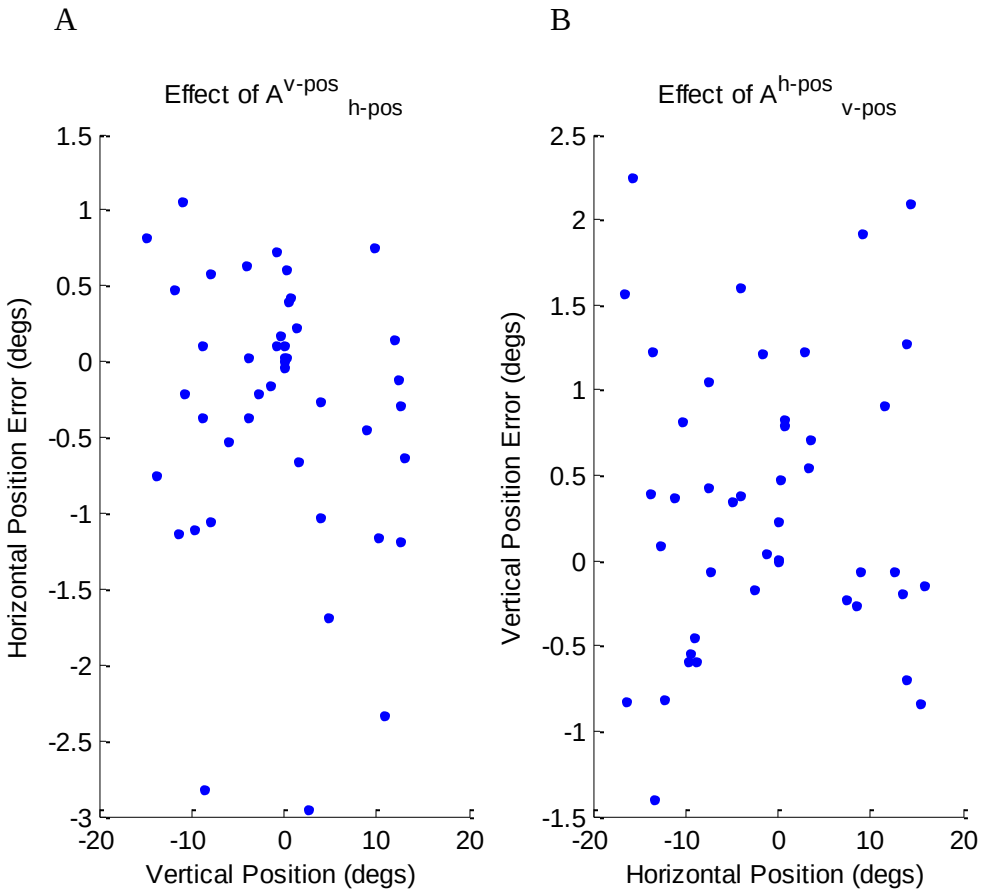

Figure 32: Interaction effects within the system based solely on position ($A^{h\text{-}pos}_{v\text{-}pos}$ and $A^{h\text{-}pos}_{v\text{-}pos}$) from the 2-D saccade task of a sample subject (EM_S08). Each dot shows the steady-state error between the absolute values of the subject gaze and target positions, computed by averaging the positional error over the duration of a target step. Positive position errors indicate subjects' gaze was more centrifugal (toward position away from center) compared to the target positions. For both interaction effects shown, the horizontal and vertical position errors did not increase systematically

as vertical and horizontal positions increased. For $A^{h\text{-}pos}_{v\text{-}pos}$, the magnitudes of the overshoots (positive position errors) and undershoots (negative position errors) tended to increase for more centrifugal horizontal positions, but the variability in the vertical errors indicate inconsistency in this effect.

An earlier study by Bahill and Stark (1975) showed horizontal position influence on vertical velocity, such that vertical velocity was decreased by 20% for a 39 degree horizontal abduction (eye movement away from center). They suggested that the effect may be due to differences in the particular muscles contributing to the two directions of movement. Anatomically, the medial and lateral recti muscles aligned on the horizontal axis of the eyeball actuate horizontal eye movements, while the inferior and superior recti muscles aligned on the vertical axis of the eyeball actuate vertical eye movements (Kandel, Schwartz, & Jessell, 2000). The inferior and superior oblique muscles are positioned diagonally on the eyeball and mainly provide torsion (rotation about line of vision) but also contribute to horizontal and vertical eye movements (Kandel et al., 2000). For the observed reduction in vertical velocity with horizontal positions, it is possible that the superior and inferior recti muscles' influence on vertical movement decreases for increasing horizontal eye eccentricities because those muscles are stretched beyond optimal functioning lengths. At high eccentricities, driving forces for the vertical eye movements may rely more on oblique muscles, and perhaps these muscle types do not generate as much force as the recti muscles.

A comparable effect was not seen in this study due to the more limited range of motion tested (±18 degrees). Instead, the best-fit models indicated that horizontal and vertical velocities increased with vertical and horizontal eccentricity. This result cannot

be compared to Bahill's observations, whose data was taken at an eccentricity (39˚) outside of the range of motion for this study (±18˚).

For the 2-D smooth-pursuit task, there was a clear effect of velocity on cross-axial position for both horizontal and vertical movements ($p<0.0001$). Specifically, an increase in speed resulted in a tendency to move to the center position along the opposite axis, resulting in oblique movements curving centripetally (towards the horizontal and vertical midlines) based on the speed of eye movements along the horizontal or vertical midlines. This may be compensated by centrifugally curved oblique movements (for both saccades and smooth-pursuit eye movements) based on the error between eye and target positions along the horizontal or vertical midlines ($B^{v\text{-}e}_{h\text{-}pos}$ and $B^{h\text{-}e}_{v\text{-}pos}$). The results suggest that centripetal curving may occur naturally as a result of system interactions, and that centrifugal curving driven by the controller may be used to correct for the resulting position errors to produce oblique movements with straighter trajectories and reduce travel distance to fixate the target. Becker and Jurgens (1990), showed that oblique saccades typically correct for early deviations from a projected straight trajectory to a target (Becker & Jurgens, 1990). For example, a saccade towards a target located directly beneath the fixation point may begin with some horizontal displacement that is corrected after movement onset resulting in a curved trajectory. The responses of the best-fit models support the interpretation of the interaction as a "correction" that acts on positional error to correct for curvature naturally induced by the ocular system.

As discussed in Section 2.5, the independent control hypothesis postulates that motor commands to control horizontal and vertical eye movements are generated independently of one another. The resultant best-fit parameters from the model suggest

interactions between the generation of motor commands for the horizontal and vertical eye movements, which contradicts the independent control hypothesis. Table 4 shows statistical significance or almost statistical significance for error-induced centrifugal curvature ($B^{v\text{-}e}_{h\text{-}pos}$ and $B^{h\text{-}e}_{v\text{-}pos}$; $p<0.055$) for both 2-D saccade and smooth-pursuit data, and with motor commands being proportional to position errors, this suggests interaction between the motor commands. The error-induced effects on velocity ($B^{v\text{-}e}_{h\text{-}vel}$ and $B^{h\text{-}e}_{v\text{-}vel}$) were generally not significant ($p>1.77$), with the exception of $B^{v\text{-}e}_{h\text{-}vel}$ from the smooth-pursuit task ($p=0.01$), perhaps due to the small sample size of the study, but the corresponding best-fit parameters were consistently negative across subjects, resulting in slower movements along the direction that requires greater eye displacement for an oblique eye movement. This effect supports the concept of component stretching, where the duration of the longer-traveling component of an oblique saccade is stretched so that the end times of the two components coincide to produce straight trajectories to the target. Overall, the presence of statistically significant interactions in the best-fit model is not generally consistent with an independent control hypothesis. The results instead support the existence of interactions that result in centrifugal curvature, based on position errors, and component stretching. However, the small effects of the significant interactions on the functional response seem to qualitatively support independent control hypothesis, and future studies may investigate which results are more valid.

5.3 Model Limitations

The oculomotor control model used in this study makes several assumptions. The ocular dynamics were modeled by a second-order system that combined the eye muscles and plant into one entity (Robinson, 1964; Robinson et al., 1986). Subsequent models

have improved on this by separating the agonist and antagonist muscles in order to improve the velocity profiles of saccades (Bahill et al., 1975b; Clark & Stark, 1976; G. Cook & L. Stark, 1968; Hsu, Bahill, & Stark, 1976). The velocity profiles, relative to time, were not investigated in this study, but a more sophisticated ocular dynamics system could be incorporated to better characterize these effects in future studies. The ocular dynamics and motor command contributions (A_1-A_4 and B_1-B_2 parameters) were also assumed to be identical for both horizontal and vertical movements. Similar assumptions have been made in other studies of oblique eye movements (Chen-Harris et al., 2008), making it unclear if the effect on horizontal and vertical movement differences occurred at the level of the controller or ocular dynamics. In the proposed model, we assumed that differences in 1-D axial movements were attributed to the controller. Future studies may individually fit the vertical ocular dynamics (A_{1y}-A_{4y}) along with the controllers, to quantify differences in ocular dynamics between horizontal and vertical eye movements. Adding these parameters to the fitting process may reduce differences between the horizontal and vertical components of the best-fit 1-D controllers and could potentially impact the interpretation of the 2-D interactions. For example, larger differences between the 1-D horizontal and vertical ocular dynamics (1-D, state matrix 'A' parameters) could further reduce the contributions of system interactions (2-D, state matrix 'A' parameters).

A second model assumption concerned the internal prediction of eye movement. The model assumed the oculomotor system completely and accurately estimated eye movements such that internal prediction of the movement completely canceled the delayed information from visual feedback. This assumption was reasonable in the

current study with visually-healthy subjects for whom the accuracy of eye movements suggests the effects of an imperfect internal plant representation was negligible. Fitting this model to subjects with visual deficits, such as those with MS, may require freeing the internal plant parameters, as this effect should not be ruled out. This will likely also add uncertainty in the estimates.

The model was also limited by the range of motion in the visual tasks: ±18 degrees of visual arc. Saccade amplitudes above this range would require subject specific estimates of the velocity saturation in the model (Figure 7 A). This may be implemented using appropriate sigmoidal or natural log equations to characterize movements within the saturation region.

In the proposed model, the smooth-pursuit control loop did not incorporate glissades, which are drifting ocular movements towards the target during the end of a saccade (Bahill, Clark, & Stark, 1975c). Instead smooth-pursuit control was implemented for position error that fell within the saccade dead zone region, rather than glissade control. Smooth-pursuit and glissade movements are both slow but may be driven by different target signals, as smooth-pursuit is mediated by a moving target while a glissade is mediated by a stationary target. Future oculomotor models may attempt to characterize glissades by incorporating PID control within the dead zone separate from the smooth-pursuit PID control, where a stationary target may be required for activation of glissade control.

Limitations in the eye tracking resolution likely contributed errors in dead zone analysis and general parametric analysis. Accurate estimation of the dead zone required detection of saccade amplitudes less than 0.5˚. Smoothing the data reduced noise from

the Arrington system used in this study, but this reduced the displacements between consecutive gaze points, resulting in lower saccade velocities.

5.4 Future Directions

5.4.1 Improving Eye Movement Characterization

The eye tracking resolution of 60 Hz is much smaller than earlier studies that used infrared eye trackers with 1000 Hz (Bahill & Stark, 1975; Chen-Harris et al., 2008; Schmitt, Muser, Lanz, Walz, & Schwarz, 2007). The low resolution contributes positional error to eye movement measurements when changes in eye position are misidentified, particularly during the 30-80 ms saccade duration in which saccades can only be represented by 1-4 data points. The lack of data points may under-characterize the curvature required to identify 2-D interactions between horizontal and vertical eye movements, and the misidentified timing of saccade movements affects velocity calculations used by the model to modulate derivative control. Thus, future studies measuring eye movements with higher resolution eye tracking systems may help confirm or reject results seen in this study.

Alternatively, sampling could be augmented by running repeating trials for each subject. Assuming ergodicity and variability of sampling onset times, this could yield better sampling for eye movements to repeated targets, effectively increasing the sampling rate. Interspersing the repeated trials within novel trials would be recommended to minimize subjects' ability to make predictive eye movements. Different eye movement measurement modalities such as the electro-oculogram could also be coupled with the infrared eye tracker to yield more data .

To avoid computational complexity, saccade control was characterized here by a general PD controller. Controller performance could be improved by utilizing a more physiologically consistent pulse-step control. Pulse-step control can be approximated by a PD control model using a high derivative gain whose maximum amplitude is saturated (Winters et al., 1984),

whereby the high derivative gain accounts for the fixed rise time of a pulse signal, while the saturation accounts for the height of the motor command. This type of controller setup (pulse-step) allows the model to produce faster saccades than a typical PD controller while maintaining stability. To illustrate the benefit, the high derivative gain with saturation PD controller was implemented for horizontal saccade control and fit to EM_S06's horizontal saccade data (randomly selected) and the controller's sensitivity and accuracy to subject data was examined. Table 7 shows the model's fit to subject data, in which the derivative gain is fixed to values larger than the initial-model value and parameters accounting for proportional control and

	Derivative Gain	Saturation Gain Initial	Saturation Gain Final	Proportional Gain	R^2 (degs)	RMSE (degs)
Fit #1	0.0418	25	41.44	6.05	0.9598	1.6218
Fit #2	0.0418	50	49.02	5.29	0.9613	1.6263
Fit #3	0.0418	75	59.65	4.47	0.9604	1.6502
Fit #4	0.0418	100	50.96	4.31	0.96	1.617
Fit #5	0.0836	25	39.91	9.18	0.9595	1.6216
Fit #6	0.0836	50	47.84	7.71	0.9589	1.612
Fit #7	**0.0836**	**75**	**47.65**	**6.5**	**0.9614**	**1.6045**
Fit #8	0.0836	100	99.99	3.73	0.9576	1.685
Fit #9	0.209	25	30.12	11.31	0.9484	1.7912
Fit #10	0.209	50	51.49	9.39	0.9439	1.8909
Fit #11	0.209	75	58.55	7.33	0.9578	1.6448
Fit #12	0.209	100	52.41	9.34	0.9606	1.6123

Table 7: Curve-fitting horizontal saccade data (from EM_S06) to modified PD controller with output saturation to model pulse-step control. The derivative gain was fixed to an arbitrary values that were factors of 1, 2 and 5 larger than the initial-model value, and the proportional and saturation gains were free for fitting. The proportional gain was pseudo-randomly perturbed using the -10 to 10 factor range about the initial conditions, while the saturation gain had systematic initial conditions of 25, 50, 75 and 100 Newton-meters for each fit. Correlation (R^2) and root mean squared error (RMSE) are shown for each fit to quantify goodness of fit between model and subject response. The sensitivity of fitting the saturation gain to the saccade data is demonstrated by the parameter's convergence to approximately 50 (±10) N-m for 10 out of the 12 fits. Fit #7 demonstrated the highest correlation and lowest error.

motor command saturation are freed for fitting. Under all tested derivative gains and initial conditions for saturation, the fitted saturation parameter drifts towards a value of 50 Newton-meters, suggesting the parameter can be fit to subject data. From the tested conditions seen in Table 7, the model performed optimally with a derivative gain set twice as large or equal to the initial-model value, with Fit #7 (saturation of 47.65 N-m and proportional gain of 6.5) having the highest correlation and lowest error. The best-fit controller from this small sample of fits were represented by values from Fit #7 and was compared to the initial-model's PD controller in Figure 33.

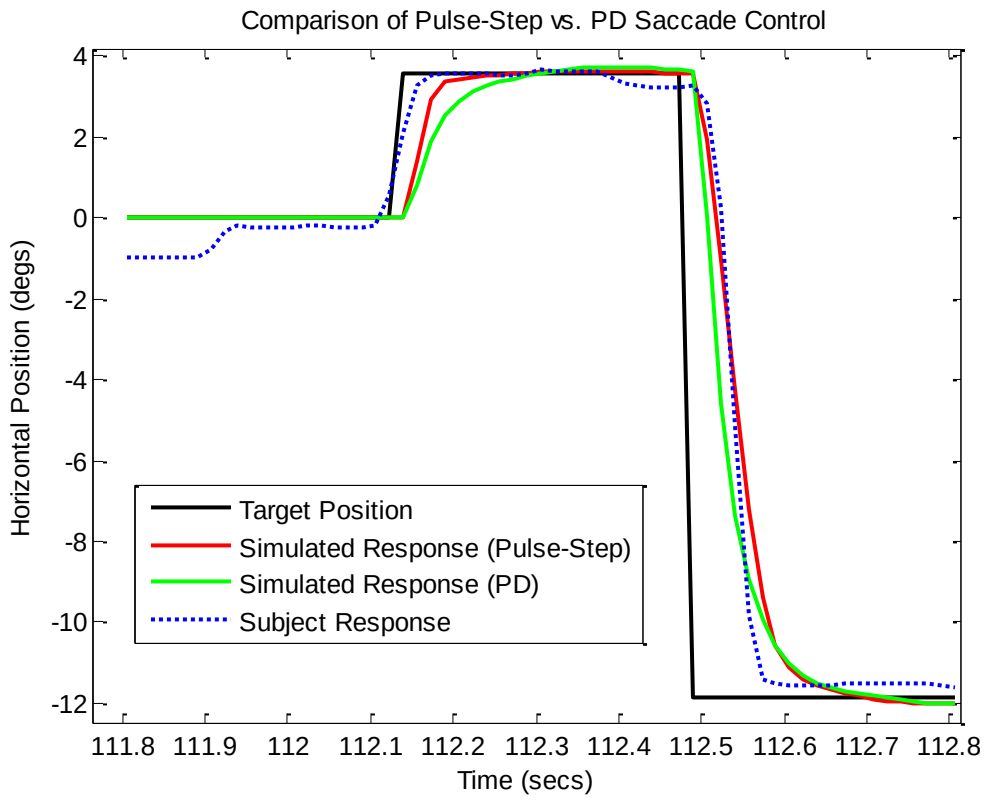

Figure 33: Comparison of Pulse-Step vs. PD saccade control. The model response using the PD controller from the initial-model (solid red) is compared with the model response using the Pulse-Step controller with proportional and saturation gains of 6.5 and 47.65 respectively (solid green). The target (solid black) and subject gaze (dotted blue) positions are example data from EM_S06. Implementing the pulse-step controller over the PD controller improved the model's ability to match the subject's saccade trajectory, as seen in the rising slope of the first target step and the falling slope of the last target step. For the first target step, the pulse-step controller showed a more critically-damped response as well, which is more consistent with the subject data.

From the figure, the pulse-step controller allowed the model to more accurately characterize the steep slope and critically-damped response from a subject's saccades versus the PD controller. The response from the pulse-step controller also showed a correlation and root mean squared error of 0.96 and 1.63 degrees between the model and subject responses, which is an improvement from the 0.95 and 1.81 degrees afforded by the PD controller.

Figure 33 shows that the saccade velocity from the best-fit pulse-step controller is lower than the subject response, so the velocity from the PD controller seems like a better fit. It should be noted that increasing the motor command saturation noticeably increases the velocity for larger steps. Figure 34 shows the effect of increasing this parameter by approximately 50% of the best-fit value, where the velocity of the simulated saccade was a better match qualitatively to the subject saccade. The correlation and error between

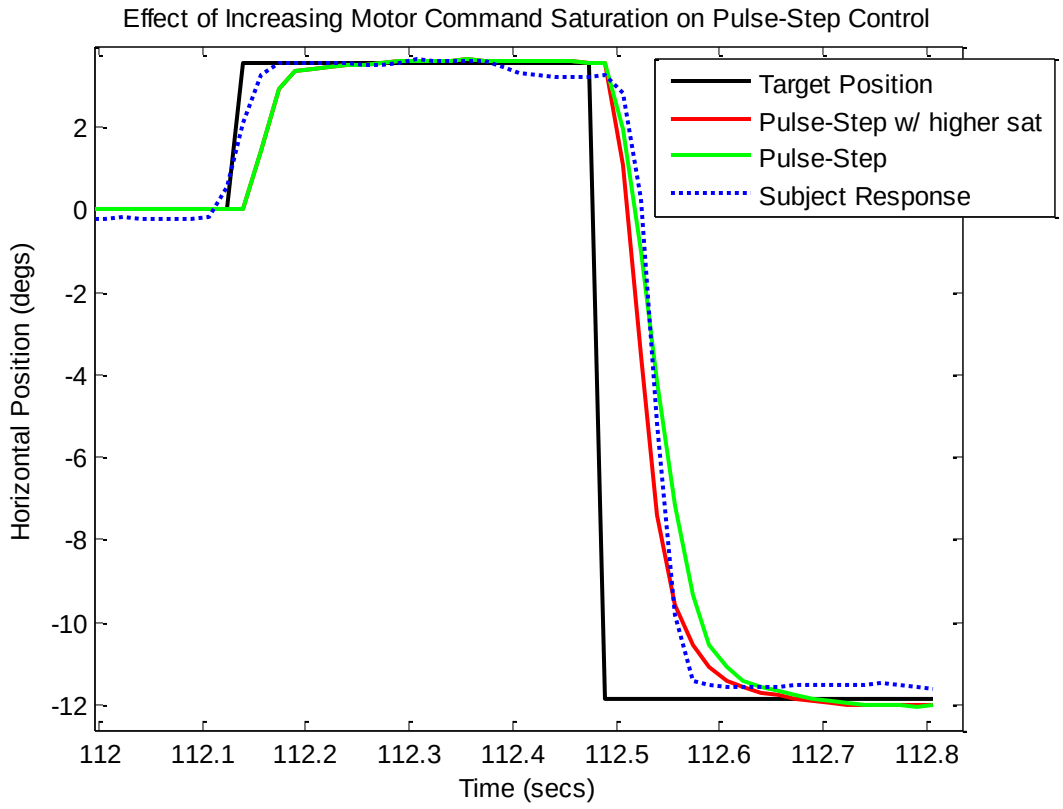

Figure 34: Effect of increasing motor command saturation on pulse-step control. The model response using the best-fit Pulse-Step controller except for a 50% increase in saturation to 75 N-m (solid red) is compared with the model response using the best-fit Pulse-Step controller which had a saturation gain of 47.65 (solid green). The target (solid black) and subject gaze (dotted blue) positions are example data from EM_S06. For the larger saccade step, the higher saturation gain increased the model's velocity, which more closely represents the subject's velocity for the first 75% of displacement (solid red vs. dotted blue) than the best-fit model with a lower saturation gain (solid green vs. dotted blue).

this controller and subject response was lower than the best-fit controller (0.9584 versus 0.9614, and 1.6988 degs versus 1.6045 degs), due to the unusually higher latency of the sample data for the subject. These results support the incorporation of a pulse-step control for future studies.

In addition to saccade control, it could be argued that some parameters characterizing interactions between horizontal and vertical eye movements can be removed based on their lack of significance (Table 3 and Table 4). However, these may

be mischaracterized by a lack of sufficient data in this study, especially when considering that only 1-4 data points were used to characterize the 2-D curvature of saccades with a 60 Hz eye tracking system. The results demonstrate that model fit to subjects' data was sensitive to a subset of interactions, but this does not preclude other forms of significant interactions whose sensitivity was negatively impacted by the eye tracking system. Upgrading the eye tracker system is a recommended priority for follow-up studies to more accurately characterize interactions. Therefore, while removing seemingly insignificant parameters may further constrain the model to improve curve-fitting, keeping the general model structure described in this study is recommended.

The influence of data preprocessing techniques on the results was not investigated here. More advanced preprocessing techniques could improve the eye tracking data and subsequent analysis for the current system. For example, the estimation of eye position during eye blinks could be improved by using a 5^{th} order spline interpolation to maintain eye velocity and acceleration continuity during the blink interval. The current study simply cuts out eye position data classified as eye blinks; this is not recommended for follow-up studies where higher resolution eye trackers will be used and more accurate eye positions are expected. Another example is the automation of artifact removal from eye tracking data to reduce the human error of visually inspecting the data, as was done in this study.

5.4.2 Eye Movement Studies in Persons with Multiple Sclerosis

Previous studies by Feys and colleagues have begun to examine the relationship between eye and arm movement deficits in MS (Feys, 2003, 2005, 2008). Using 1-D wrist tracking and finger aiming tasks, their studies attempted to characterize the effects

of oculomotor deficits on manual movement by examining movements in the presence and absence of visual information as subjects performed goal-directed tasks. They found correlation between initiation phase durations (time between visual target and onset of eye or hand movement) and directional changes between ballistic eye and hand movements for both MS and control subjects (Feys, 2003). When visual information about the movement was available, eye and hand movements during stabilization exhibited a larger range in amplitudes compared to the condition where the subjects' arm was hidden (Feys, 2003). In a later study, Feys found that intention tremor during wrist tracking decreased when the subjects' initial saccade (rapid, intermittent eye movements) to the target (first saccade reacting to a target step) decreased (Feys, 2005). Error-corrective movements decreased when the initial saccades decreased as well. Their results suggest that eye movements affect the accuracy of arm movements. However, the relationship between visual information and intention tremor was not shown to be causal.

This study focused on oculomotor control in healthy subjects. Including persons with MS may reveal characteristic changes between the two groups, reflecting differences in control strategies for goal-directed ocular movements. In addition, this model can be incorporated into existing sensorimotor control models to integrate ocular and arm movements to understand the relationship between these two systems across different patient populations.

6. CONCLUSION

The three aims for this study were met. A stabilized oculomotor control model was developed and the sensitivity of the model to characterize saccades and smooth-pursuit eye movements in visually-healthy subjects was quantified. A system identification process was developed to systematically acquire subject-specific parameters for the oculomotor control model using 1-D saccade, 1-D smooth-pursuit and 2-D saccade and smooth-pursuit data. The model was evaluated using test data with a 2.987˚ (±0.252) and 2.627˚ (±0.210) root mean squared error for the horizontal and vertical eye movements respectively. Higher temporal and spatial resolutions of eye tracker systems used in future studies may improve the fitting accuracy of the system identification process. The 2-D analysis of eye movements in this study suggested interactions between horizontal and vertical oculomotor control that induce centrifugal curvature and component stretching, but the typically small functional effects qualitatively suggest an independent control hypothesis.

BIBLIOGRAPHY

Abrams, R. A., Meyer, D. E., & Kornblum, S. (1989). Speed and accuracy of saccadic eye movements: characteristics of impulse variability in the oculomotor system. ***J Exp Psychol Hum Percept Perform, 15*****(3), 529-543.**

Arrington. Scene Camera Eye Tracking, 2013, from http://www.arringtonresearch.com/scene.html

Bahill, A. T., Clark, M. R., & Stark, L. (1975a). Computer simulation of overshoot in saccadic eye movements. ***Computer Programs in Biomedicine, 4*****, 230-236.**

Bahill, A. T., Clark, M. R., & Stark, L. (1975b). Dynamic overshoot in saccadic eye movements is caused by neurological control signed reversals. ***Exp Neurol, 48*****(1), 107-122.**

Bahill, A. T., Clark, M. R., & Stark, L. (1975c). Glissades are generated by mismatched components of the saccadic motoneuronal control signal. ***Mathematical Biosciences*****.**

Bahill, A. T., & McDonald, J. D. (1983). Model emulates human smooth pursuit system producing zero-latency target tracking. ***Biol Cybern, 48*****(3), 213-222.**

Bahill, A. T., & Stark, L. (1975). Overlapping saccades and glissades are produced by fatigue in the saccadic eye movement system. ***Exp Neurol, 48*****(1), 95-106.**

Bahill, A. T. C., M.R.; Stark, L. (1975). The main sequence, a tool for studying human eye movements. ***Mathematical Biosciences*****, 191-204.**

Bahill, A. T. S., L. (1975). Neurological control of horizontal and vertical components of oblique saccadic eye movements. . ***Mathematical Biosciences*****, 287-298.**

Balkenius, C., & Johansson, B. (2005, 2005). ***Event prediction and object motion estimation in the development of visual attention.*** **Paper presented at the Fifth International Workshop on Epigenetic Robotics, Nara, Japan.**

Baloh, R. W., Yee, R. D., Honrubia, V., & Jacobson, K. (1988). A comparison of the dynamics of horizontal and vertical smooth pursuit in normal human subjects. ***Aviat Space Environ Med, 59*****(2), 121-124.**

Becker, W., & Jurgens, R. (1990). Human oblique saccades: quantitative analysis of the relation between horizontal and vertical components. ***Vision Res, 30*****(6), 893-920.**

Bridgeman, B. (2007). Efference copy and its limitations. ***Comput Biol Med, 37*****(7), 924-929. doi: 10.1016/j.compbiomed.2006.07.001**

Brown, C. (1989). Prediction in gaze and saccade control (pp. 39). Rochester, NY: University of Rocherster.

Chen-Harris, H., Joiner, W. M., Ethier, V., Zee, D. S., & Shadmehr, R. (2008). Adaptive control of saccades via internal feedback. ***J Neurosci, 28*****(11), 2804-2813. doi: 10.1523/JNEUROSCI.5300-07.2008**

Clark, M. R., & Stark, L. (1976). Sensitivity of control parameters in a model of saccadic eye tracking and estimation of resultant nervous activity. ***Bull Math Biol, 38*****(1), 39-57.**

Collewijn, H., Erkelens, C. J., & Steinman, R. M. (1988a). Binocular co-ordination of human horizontal saccadic eye movements. ***J Physiol, 404*****, 157-182.**

Collewijn, H., Erkelens, C. J., & Steinman, R. M. (1988b). Binocular co-ordination of human vertical saccadic eye movements. ***J Physiol, 404*****, 183-197.**

Collins, T., Semroud, A., Orriols, E., & Dore-Mazars, K. (2008). Saccade dynamics before, during, and after saccadic adaptation in humans. ***Invest Ophthalmol Vis Sci, 49*****(2), 604-612. doi: 10.1167/iovs.07-0753**

Cook, G., & Stark, L. (1968). Dynamic behavior of human eye-positioning mechanism. ***Communications in behavioral biology, 1*****, 197-204.**

Cook, G., & Stark, L. (1968). The human eye-movement mechanism. Experiments, modeling, and model testing. ***Arch Ophthalmol, 79*****(4), 428-436.**

de Brouwer, S., Yuksel, D., Blohm, G., Missal, M., & Lefevre, P. (2002). What triggers catch-up saccades during visual tracking? ***Journal of Neurophysiology, 87*****(3), 1646-1650. doi: DOI 10.1152/jn.00432.2001**

Erkelens, C. J. (2006). Coordination of smooth pursuit and saccades. ***Vision Res, 46*****(1-2), 163-170. doi: 10.1016/j.visres.2005.06.027**

Feys, P., Helsen, W., Nuttin, B., Lavrysen, A., Ketelaer, P., Swinnen, S., & Liu, X. (2008). Unsteady gaze fixation enhances the severity of MS intention tremor. ***Neurology, 70*****(2), 106-113. doi: 10.1212/01.wnl.0000287071.51180.b1**

Feys, P., Helsen, W. F., Lavrysen, A., Nuttin, B., & Ketelaer, P. (2003). Intention tremor during manual aiming: a study of eye and hand movements. ***Mult Scler, 9*****(1), 44-54.**

Feys, P., Helsen, W. F., Liu, X., Lavrysen, A., Loontjens, V., Nuttin, B., & Ketelaer, P. (2003). Effect of visual information on step-tracking movements in patients with intention tremor due to multiple sclerosis. ***Mult Scler, 9*****(5), 492-502.**

Feys, P., Helsen, W. F., Liu, X., Nuttin, B., Lavrysen, A., Swinnen, S. P., & Ketelaer, P. (2005). Interaction between eye and hand movements in multiple sclerosis patients with intention tremor. ***Mov Disord, 20*****(6), 705-713. doi: 10.1002/mds.20382**

Forster, J. D., Van Houtte, N., & Young, L. R. (1969). A revised stochastic sampled data model for eye tracking movements. ***Nasa TechDocs*****.**

Freedman, E. G., & Cecala, A. L. (2008). Oblique gaze shifts: head movements reveal new aspects of component coupling. ***Prog Brain Res, 171*****, 323-330. doi: 10.1016/S0079-6123(08)00647-X**

Grossman, G. E., & Robinson, D. A. (1988). Ambivalence in modelling oblique saccades. ***Biol Cybern, 58*****(1), 13-18.**

Hsu, F. K., Bahill, A. T., & Stark, L. (1976). Parametric sensitivity analysis of a homeomorphic model for saccadic and vergence eye movements. ***Comput Programs Biomed, 6*****(2), 108-116.**

Kandel, E. R., Schwartz, J. H., & Jessell, T. M. (2000). ***Principles of Neuroscience*** **(4th ed.): McGraw-Hill.**

Kapoula, Z., & Robinson, D. A. (1986). Saccadic undershoot is not inevitable: saccades can be accurate. ***Vision Res, 26*****(5), 735-743.**

Krauzlis, R. J., & Lisberger, S. G. (1994). A model of visually-guided smooth pursuit eye movements based on behavioral observations. ***J Comput Neurosci, 1*****(4), 265-283.**

Lesmana, M. D., P,K. (2011). ***A Biologically Inspired Controller For Fast Eye Movements*****. Paper presented at the IEEE International Conference on Robotics and Automation, Shanghai, China.**

Lisberger, S. G., Evinger, C., Johanson, G. W., & Fuchs, A. F. (1981). Relationship between eye acceleration and retinal image velocity during foveal smooth pursuit in man and monkey. ***Journal of Neurophysiology, 46*****(2), 229-249.**

Meyer, C. H., Lasker, A. G., & Robinson, D. A. (1985). The upper limit of human smooth pursuit velocity. ***Vision Res, 25*****(4), 561-563.**

Miall, R. C., Weir, D. J., Wolpert, D. M., & Stein, J. F. (1993). Is the cerebellum a smith predictor? ***J Mot Behav, 25*****(3), 203-216. doi: 10.1080/00222895.1993.9942050**

Nichols, M. J., & Sparks, D. L. (1996). Independent feedback control of horizontal and vertical amplitude during oblique saccades evoked by electrical stimulation of the superior colliculus. ***Journal of Neurophysiology, 76*****(6), 4080-4093.**

Orban de Xivry, J. J., & Lefevre, P. (2007). Saccades and pursuit: two outcomes of a single sensorimotor process. ***J Physiol, 584*****(Pt 1), 11-23. doi: 10.1113/jphysiol.2007.139881**

PNNL. (2008, 07/2008). Calculations for Assessing Data Quality Retrieved 10/15/2013, 2013, from http://agg.pnnl.gov/docs/conducting-work/ex22.stm

Purves, D. A., G.J.; Fitzpatrick, D. (2001). Types of Eye Movements and Their Functions ***Neuroscience*****. Sunderland, MA: Sinauer Associates.**

Quaia, C., & Optican, L. M. (1997). Model with distributed vectorial premotor bursters accounts for the component stretching of oblique saccades. ***Journal of Neurophysiology, 78*****(2), 1120-1134.**

Rashbass, C. (1961). The relationship between saccadic and smooth tracking eye movements. ***J Physiol, 159*****, 326-338.**

Robinson, D. A. (1964). The Mechanics of Human Saccadic Eye Movement. ***J Physiol, 174*****, 245-264.**

Robinson, D. A. (1975). A quantitative analysis of extraocular muscle cooperation and squint. ***Invest Ophthalmol, 14*****(11), 801-825.**

Robinson, D. A., Gordon, J. L., & Gordon, S. E. (1986). A model of the smooth pursuit eye movement system. ***Biol Cybern, 55*****(1), 43-57.**

Rottach, K. G., Zivotofsky, A. Z., Das, V. E., Averbuch-Heller, L., Discenna, A. O., Poonyathalang, A., & Leigh, R. J. (1996). Comparison of horizontal, vertical and diagonal smooth pursuit eye movements in normal human subjects. ***Vision Res, 36*****(14), 2189-2195.**

Rovati, G. E. (1990). A versatile implementation of the Gauss-Newton minimization algorithm using MATLAB for Macintosh microcomputers. ***Comput Methods Programs Biomed, 32*****(2), 161-167.**

Schmidt-Cornelius, H. (2002). ***Reverse engineering an active eye.*** **Ph.D. , University of Sussex.**

Schmitt, K. U., Muser, M. H., Lanz, C., Walz, F., & Schwarz, U. (2007). Comparing eye movements recorded by search coil and infrared eye tracking. ***J Clin Monit Comput, 21*****(1), 49-53. doi: 10.1007/s10877-006-9057-5**

Thomas, J. G. (1969). The dynamics of small saccadic eye movements. ***J Physiol, 200*****(1), 109-127.**

van Gisbergen, J. A., van Opstal, A. J., & Schoenmakers, J. J. (1985). Experimental test of two models for the generation of oblique saccades. ***Exp Brain Res, 57*****(2), 321-336.**

Vercher, J. L., Quaccia, D., & Gauthier, G. M. (1995). Oculo-manual coordination control: respective role of visual and non-visual information in ocular tracking of self-moved targets. ***Exp Brain Res, 103*****(2), 311-322.**

Wakde, S. (2011). ***Asymmetric Transfer of Task Dependent Perceptual Learning in Visual Motion Processing.*** **Masters, Marquette University, Milwaukee, WI.**

Westheimer, G. (1954). Mechanism of saccadic eye movements. ***AMA Arch Ophthalmol, 52*****(5), 710-724.**

Winters, J. M., Nam, M. H., & Stark, L. W. (1984). Modeling Dynamical Interactions between Fast and Slow Movements - Fast Saccadic Eye-Movement Behavior in the Presence of the Slower Vor. ***Mathematical Biosciences, 68*****(2), 159-185. doi: Doi 10.1016/0025-5564(84)90030-0**

Yang, Q., Bucci, M. P., & Kapoula, Z. (2002). The latency of saccades, vergence, and combined eye movements in children and in adults. ***Invest Ophthalmol Vis Sci, 43*****(9), 2939-2949.**

Yee, R. D., Schiller, V. L., Lim, V., Baloh, F. G., Baloh, R. W., & Honrubia, V. (1985). Velocities of vertical saccades with different eye movement recording methods. ***Invest Ophthalmol Vis Sci, 26*****(7), 938-944.**

Young, L. R. (1971). Pursuit Eye Tracking Movements. In P. Bach-y-Rita, C. C. Collins & J. E. Hyde (Eds.), ***Control of Eye Movements*** **(pp. 429-443). New York: Academic Press.**

Young, L. R. S., L. (1963). Variable feedback experiments testing a sampled data model for eye tracking movements. ***IEEE Transactions on Human Factors in Electronics*****, 38-51.**